Escola de Camins
Escola Tècnica Superior d'Enginyeria de Camins, Canals i Ports
UPC BARCELONATECH

PROJECTE O TESINA D'ESPECIALITAT

Títol

Power generation from tidal currents.

Application to Ria de Vigo

711-TES-CA-6797

Autor/a

Maria Griño Colom

Tutor/a

Juan Pablo Sierra Pedrico

Octavio Cesar Mösso Aranda

Marc Mestres Ridge (tutor extern)

Departament

Departament d'Enginyeria Hidràulica, Marítima i Ambiental (DEHMA)

Intensificació

Data

19 de maig de 2015

I would like to express my sincere gratitude to my three thesis supervisors, Joan Pau Sierra, Cesar Mösso and Marc Mestres, for their continuous support and guidance during this thesis work. I am also indebted to Rosa López for her unconditional help and to Asunción López for putting up with me during the lasts months of stress. Lastly, my deepest thanks to my family for encouraging me when I really need it and for accepting me always.

“El que no se embarca no se marea”

(Anonymous)

Abstract

Tidal current energy, which harnesses the kinetic energy contained in the tidal streams, is emerging as a great potential energy source. It has a number of advantages with regard to other renewable energies. The resource predictability, the minimal visual impact and land occupation, its high load factor, its sustainability, etc. are some of the noteworthy features.

Contrariwise, the development of tidal current power industries is still at an early stage. Tidal energy devices are prototypes and academics, investors, industries and governments seek for identifying the best device to approach the commercial stage in terms of cost of energy and performance.

The Ría de Vigo, a large coastal embayment located in the north-west of Spain, seems to be an attractive location for evaluating the capability of tidal current power production.

The numerical model ROMS-AGRIF has been implemented in order to quantify the tidal current power potential in the Ría de Vigo and to assess the feasibility of a tidal plant. The area of study has proved to be a suitable zone comprising velocities beyond 2 m/s. The choice of the best location for tidal energy exploitation has been carried out as well as the basic design of a tidal turbine array deployment at the site.

Resumen

La energía de las corrientes marinas, la cual aprovecha la energía cinética contenida en las corrientes de marea, se perfila como una fuente de energía de gran potencial. Este recurso energético tiene una serie de ventajas con respecto a otras energías renovables. La previsibilidad de los recursos, el mínimo impacto visual y mínima ocupación de la tierra, su factor de alta carga, la sostenibilidad de un recurso inagotable, etc. son algunas de sus características destacables.

Por el contrario, el desarrollo de la industria energética de las corrientes de marea se encuentra todavía en una etapa temprana. La mayoría de los dispositivos de conversión de energía de las mareas son aún prototipos. Académicos, inversores, industrias y gobiernos tratan de identificar el mejor dispositivo para acercarse a la fase comercial en términos de coste y rendimiento de la energía.

La Ría de Vigo, una gran ensenada costera situada en el noroeste de España, parece ser un lugar atractivo para evaluar la capacidad de producción de energía de las corrientes de marea.

El modelo numérico ROMS-AGRIF se ha implementado con el fin de cuantificar el potencial energético de la Ría de Vigo y de evaluar la viabilidad de una planta mareomotriz. Se ha demostrado que el área de estudio es una zona adecuada comprendiendo velocidades más allá de 2 m/s. La elección de la mejor ubicación para la explotación de la energía de las mareas se ha llevado a cabo, así como el diseño básico del despliegue de un conjunto de turbinas mareomotrices en el lugar.

Resum

L'energia dels corrents marins, la qual aprofita l'energia cinètica continguda en els corrents de marea, emergeix com una font d'energia de gran potencial. Aquest recurs energètic té una sèrie d'avantatges respecte a altres energies renovables. La predicibilitat dels recursos, el mínim impacte visual i mínima ocupació de la terra, el seu factor d'alta càrrega, la sostenibilitat d'un recurs inesgotable, etc. són algunes de les seves característiques destacables.

Per contra, el desenvolupament de la indústria energètica dels corrents de marea es troba encara en una etapa primerenca. La majoria dels dispositius de conversió d'energia de les marees són encara prototips. Acadèmics, inversors, indústries i governs tracten d'identificar el millor dispositiu per acostar-se a la fase comercial en termes de cost i rendiment de l'energia.

La Ria de Vigo, una gran ancorada costanera situada al nord-oest d'Espanya, sembla ser un lloc atractiu per avaluar la capacitat de producció d'energia de les corrents de marea.

El model numèric ROMS-AGRIF s'ha implementat per tal de quantificar el potencial energètic de la Ria de Vigo i d'avaluar la viabilitat d'una planta mareomotriu. S'ha demostrat que l'àrea d'estudi és una zona adequada comprenent velocitats més enllà de 2 m/s. L'elecció de la millor ubicació per a l'explotació de l'energia de les marees s'ha dut a terme, així com el disseny bàsic del desplegament d'un conjunt de turbines mareomotrius en el lloc.

Table of contents

List of figures

List of tables

List of abbreviations

REP	Renewable Energy Plan
ROMS	Regional Ocean Modelling System
UCLA	University of California, Los Angeles
IRD	Institut de Recherche pour le Developpement
HF-RADAR	High-Frequency Radar
HADCP	Horizontal Acoustic Doppler Current Profiler
CDT	Conductivity, Temperature, and Depth profiles
WGS 84	World Geodetic System 1984
TEC	Tidal Energy Convertors
APD	Average Power Density (kW/m^2)
AVM	Average Velocity Module (m/s)
HATCT	Horizontal Axis Tidal Current Turbine
MCT	Marine Current Turbines
AEP	Annual Energy Production (MWh/year)
SIF	Significant Impact Factor
RTT	Rotech Tidal Turbine
ROV	Remote Operated Vehicle
O&M	Operational and Maintenance
IRR	Rate of Return
NPV	Net Present Value

Chapter I

Introduction and Objectives

The worldwide energy demand is constantly increasing due to the evolution of modern society [1]. Conventional energy sources, such as oil, gas, coal, and nuclear, are either at or nearing the limits of their ability to grow in annual supply, and will dwindle as the decades go forward. The depletion of fossil fuel reserves, global warming due to CO_2 emissions, the spread of health problems and political tensions are some of the reasons why renewable energy should be promoted. The switch to renewable energy sources should be done while fostering an evolution of personal, institutional and national values, which recognise the ultimate limits of the Earth's carrying capacities, presently being dramatically exceeded.

In Spain, renewable energies represent 14.2% of the primary energy [2]. Despite this percentage is still far from the 20% renewable energy objective proposed by the European Union for 2020 [3], the Spanish authorities estimate that the share of renewable energies will reach 22.7% by 2020. To achieve this goal, the Spanish Government has elaborated a 2011-2020 Renewable Energy Plan (REP) with the aim of promoting the development of sustainable energy projects [4].

In terms of renewable electric generation, Spain is one of the world's biggest producers of wind power (*Figure 1.1*), and also an important producer of hydraulic and solar power [5]. Nonetheless, in the last few years there has been an increase of interest in marine energies [6]. The seas and oceans offer immense open spaces where new energy technology could be set up in order to avoid land-use conflicts caused by the limitations of the renewable energy technologies based in land [7].

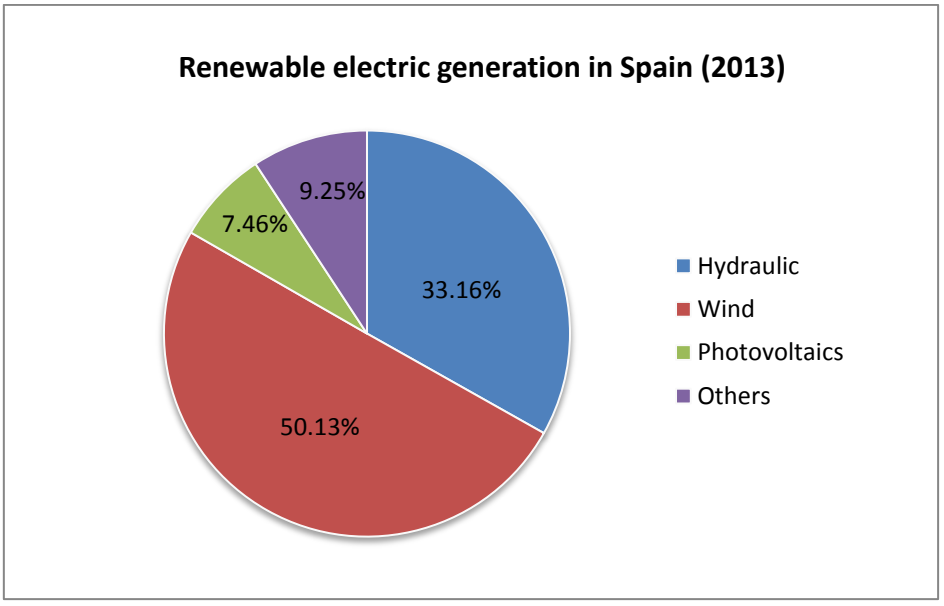

Figure 1.1: Renewable electric generation in Spain. Source: [5]

Spain has a high potential to develop marine energy technology, in particular in the Cantabrian and Atlantic Coasts and in the Canary Islands. Approximately the capacity of harnessing this energetic resource is estimated in more than 20,000 MW that would contribute to the national electric production [2]. Moreover, the REP has set the objective of implanting 100 MW of marine energy power by 2020 [8]**.**

Among marine energy sources, tidal current energy, which harness the kinetic energy contained in the tidal streams, is emerging as a great potential energy source [9]. Tidal currents are generated in the coastal regions by the rise and fall of the tides. The vertical motion of the tides near the shore causes water to move horizontally, creating tidal streams which are concentrated in areas where sea flows are channelled around or through constraining topographies such as islands and straits [10]. Furthermore, tidal current power has multiple advantages: (i) great energy potential not yet fully exploited; (ii) the resource is highly predictable unlike other renewable energy sources, such as wind or wave energy, being generated by the gravitational interaction moon-earth; (iii) minimal visual impact and land occupation since tidal power devices are fully or nearly completely submerged in water offshore, unlike the approximately 5 times bigger offshore wind turbines [11]; (iv) high load factor compared with wind power because water density is about 1000 times air density; (v) nonexistence of extreme flows, common in wind power, that could harm the tidal device; (vi) sustainable and environmentally friendly, the power of the tides is an unlimited energy resource and tidal power creates no greenhouse gas emissions or water pollutants.

Conversely, the development of tidal current power industries is still at an early stage. Tidal energy devices are prototypes and academics, investors, industries and governments seek for identifying the best device to approach the commercial stage in terms of cost of energy and performance [12]**.**

In this context, the assessment of the possibilities of harnessing tidal current power in areas where tidal flows are significant is more than justified. Following the basic site selection criterion of a minimum tidal flow peak velocity of 1.5 m/s [13], the Ría de Vigo (*Figure 1.2*), the southernmost of the four Rías Baixas, in Galicia, in the north-west of Spain, seems to be an attractive location for evaluating the capability of tidal current power production.

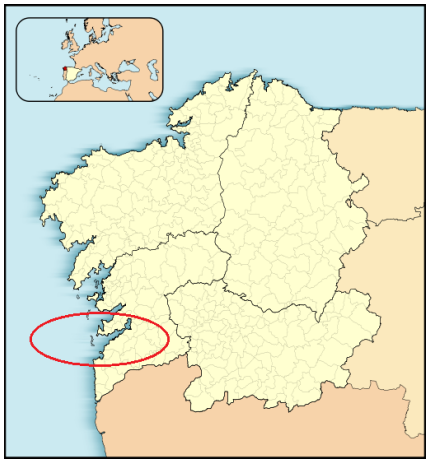

Figure 1.2: Location of the Ría de Vigo

1. Introduction and objectives

The main objective of this study is the assessment of the tidal current power potential in the Ría de Vigo. Other specific objectives are:

- To analyse the tidal current distribution within the Ría de Vigo.
- To compute the tidal power distribution within this embayment.
- To determine the best locations for tidal current turbine deployment.
- To propose a practical application for a turbine array deployment at this place.

To that end, the present work has been structured in different chapters which adopt the following contents:

Chapter 2: Performs an overview on the marine energies and, specifically, of the tidal current energy. Revision of the state of the art.

Chapter 3: Describes the study area.

Chapter 4: Presents de available data and the methodology used.

Chapter 5: Assesses the tidal energy resource in the study area.

Chapter 6: Proposes a practical application for a turbine array deployment.

Chapter 7: Presents the conclusions.

Chapter II

Background on tidal energy

2.1. Marine energies: thermal, wave and tidal energy

Oceans cover more than 70% of Earth's surface and represent a vast and large unexploited source of energy which, using different technologies, can be transformed into electricity and might help meet current energy needs.

Marine energy refers to the energy carried by ocean waves, tides, salinity and ocean temperature gradient. The three most well-developed generating technologies for deriving electrical power from the ocean are tidal power, wave power and ocean thermal energy conversion (OTEC).

The sun's heat warms the surface water greater than the deep ocean water, and this temperature difference creates the ocean's naturally available temperature gradient, or thermal energy. OCET generates enough power to justify its commercial viability if the temperature gradient is greater than 20ºC across the depth of the ocean. The technology is therefore viable primarily in equatorial areas [14].

Ocean mechanical energy is quite different from ocean thermal energy. Even though the sun affects all ocean activity, tides are driven primarily by the gravitational interaction with the Moon and Sun, and Earth's rotation, and waves are driven primarily by the winds blowing over the surface of the sea.

Regarding to wave power, the size of the waves generated will depend upon the wind speed and its duration, the distance of water over which it blows, the bathymetry of the seafloor and the currents. The resultant movement of water carries kinetic energy which can be harnessed by wave energy converters. The best wave resources occur in areas where strong winds have travelled over long distances. Nearer the coastline, wave energy decreases due to friction with the seabed, therefore waves in deeper and well exposed waters offshore will have the greatest energy. There are many designs being pursued by developers to harness the power of waves (point absorbers, attenuators, oscillating wave surge converters, oscillating water column, overtopping devices, submerged pressure differential, etc.). Wave energy resource assessments have been carried out on Spanish coasts [15] and islands [16][17]. Organizations and universities around the world are currently researching and developing new technology to harness wave energy in order to reach its commercial stage.

The present study focuses in tidal power energy and assesses the resource potential of the Ría de Vigo. The following sections give an overview of tidal energy and, specifically, of tidal current (or stream) energy.

2.2. Tidal power principles

Tides are the periodic motion of the water of the sea due to changes in the attraction forces of the Moon and Sun upon the rotating Earth.

The rise and fall of tide generates a horizontal movement of the water called tidal current. The tide rises and falls and the tidal current floods and ebbs. The range and time of the tide affect ship access to shallow ports. The time, speed and direction of the tidal current will affect the position, speed and course of a ship. Tides are superimposed on non-tidal rising and falling water levels, caused by weather, seismic events, or other natural forces. Similarly, tidal currents are superimposed upon non-tidal currents such as normal river flows, floods, and freshets.

Tides are not homogeneous on the globe. Their parameters (amplitude, period, etc.) vary from one place to another depending on complex parameters (bathymetry, geometry coastal, Coriolis forces). *Figure 2.1* shows a map of the global tidal range.

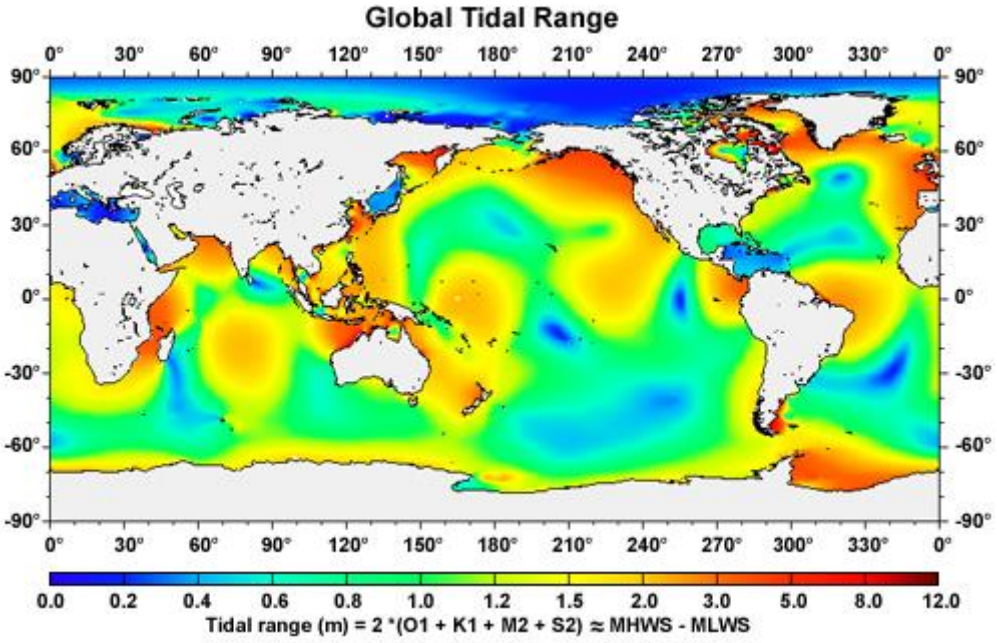

Figure 2.1: Global tidal range. Source: [18]

A tide is generated due to the gravitational force of the Sun and Moon on the Earth and the centrifugal force produced by the rotation of the Earth and Moon around each other. The gravitational force that mutually attracts any two bodies is directly proportional to the product of their masses and is inversely proportional to the square of the distance that separates the masses [19]. The attractive force exerted by the sun or moon on a water body can be calculated as:

$$F = G\frac{Mm}{d^2} \tag{2.1}$$

Where *F* (N) is the attraction force, *G* = $6.67 \cdot 10^{-11}$ ($\frac{Nm^2}{kg^2}$) is the universal constant of gravitation, *M* (kg) is the mass of the Moon or sun, *m* (kg) is the mass of a water body and *d* is the distance from a water molecule to the Moon/Sun.

The effect of the gravitational force exerted by the Sun on the Earth is about 46% of the exerted by the Moon due to the larger distance between the Earth and the Sun compared to the distance between the Earth and the Moon. Even though the Sun is much more massive, it is also much farther away.

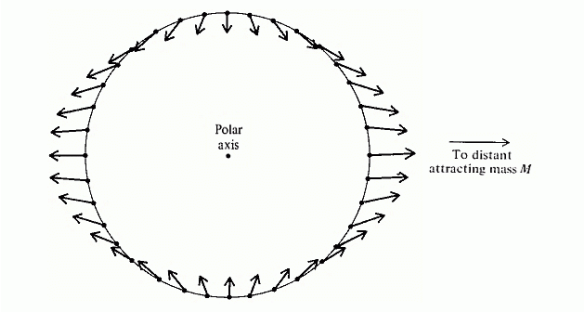

Figure 2.2: Tidal generating forces based on Earth-Moon interaction. Source: [20]

Gravitational attraction forces create two bulges in Earth's ocean envelope: one bulge on the side of the Earth facing the Moon, and the other bulge on the opposite side of the Earth (*Figure 2.2*). Rotation of the Earth within these bulges results in one or two tides (high water to low water sequence) per day, depending on Earth's latitude. The number of tides per day is related to the declination of Moon's orbital plane relative to Earth's axis of rotation. There are three different types of tidal phenomena at different locations of the earth (*Figure 2.3*); semi-diurnal tides, diurnal tides and mixed tides.

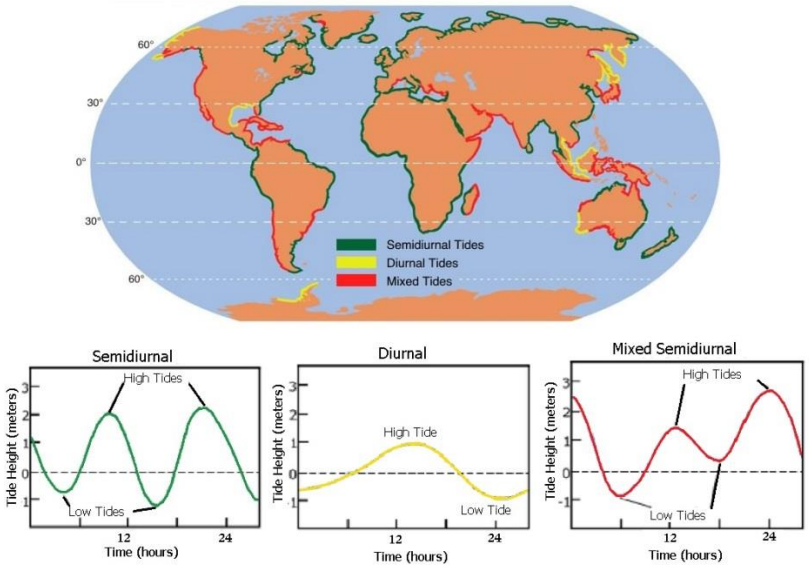

Figure 2.3: Global Distribution of Tidal Regimes. Source: [21]

Semidiurnal tides: two high and two low waters each tidal day, with relatively small differences in the respective highs and lows. It is the dominant tidal pattern in most of the world's oceans.

Diurnal tides: only one single high and single low water occur each tidal day. Tides of the diurnal type occur along the northern shore of the Gulf of Mexico, in the Java Sea, the Gulf of Tonkin, and in some other localities.

Mixed tides: combine the characteristics of diurnal and semidiurnal tides. The tide is characterized by a large inequality in the high water heights, low water heights, or in both. There are usually two high and two low waters each day, but occasionally the tide may become diurnal. Such tides are prevalent along the Pacific coast of the United States and in many other parts of the world.

As aforementioned, the amplitude of the solar tidal bulges is only 46% as high as the lunar tidal bulges. While the lunar bulges migrate around the Earth once every 27 days, the solar bulges migrate around the Earth once every day. During full moon and new moon, Sun, Moon and Earth are in line whether pulling on the same side or on the opposite side, then the gravitational attraction combine together and the tide's range reaches its maximum; the spring tide. Conversely, when Sun and Moon are orthogonal, their gravitational forces pull water in different directions and cancel each other and tide's range reaches its minimum; the neap tide. In terms of tidal power generation, the maximum power is produced during spring tide while the minimum is produced during the neap tide. *Figure 2.4* pictures the range variation of the tides during a moon cycle.

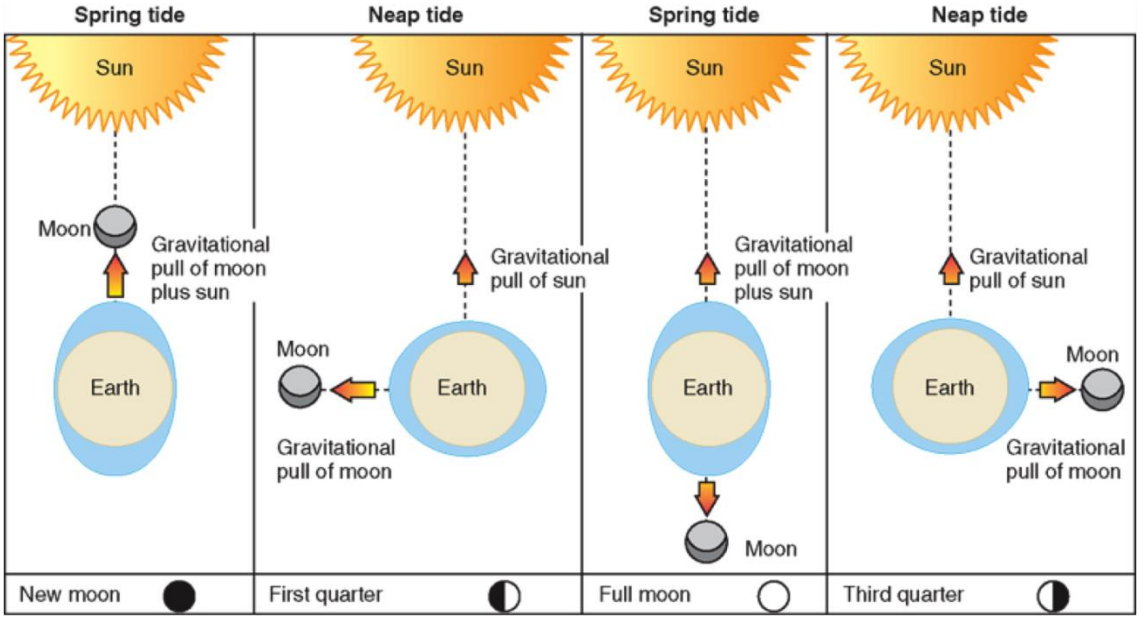

Figure 2.4: Moon phases causing spring and neap tides. Source: [22]

Tidal currents are the periodic horizontal flows of water accompanying the rise and fall of the tide. When the tide rises, from low tide to high tide, the water velocity increases causing flood currents till the water reaches its highest level. Then, it starts to decrease its velocity till the moment when the tidal current ceases, which is called slack water. The tide then reverses its direction and starts falling increasing again its velocity and

producing ebb currents till the water stops falling and reaches low tide, then velocity decrease till its minimum. *Figure 2.5* represents the velocity variation of a semidiurnal tidal current.

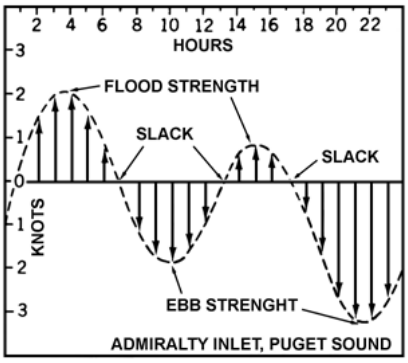

Figure 2.5: Velocity variation (in knots) of a semidiurnal tidal current. Source:[19]

Tidal currents occur in coastal areas and in places where the seabed forces the water through relatively narrow boundaries.

Tidal variations, rise-fall and flood-ebb currents, can be utilized to generate electricity, either harnessing its potential energy in tidal barrages or its kinetic energy in tidal stream devices. Next section describes both approaches.

2.3. Tidal energy types: barrage approach & tidal current approach

Although is not yet widely used, tidal power is one of the oldest forms of renewable energy used by humankind. Tide mills have been used since the 6th century [23] on the British, French and Spanish coasts. They consisted in a storage pond behind a dam that was filled during the flood through sluice gates and then emptied at the ebb through a water wheel to mill grain. The idea of generating electric power from exploiting the power of the tides was not introduced until the 19th century [24]. In 1967, the world's first large-scale tidal power plant, La Rance Barrage, was successfully completed. It has a capacity of 240 MW and it is located on the estuary of the Rance River, in Brittany, France [25].

There are principally two methods to generate electricity from the tides; to harness the potential energy of the rise and fall of the tides by building a barrage across an embayment or an estuary in high tide areas, or to extract the kinetic energy from free flowing currents occurred during floods and ebbs. Tidal power facilities can be categorized into two main types: tidal barrages and tidal current systems.

2.3.1. Tidal barrages

The technology required to convert tidal range into electricity is very similar to conventional hydroelectric power plants. Tidal barrages use the potential energy in the difference in height between high and low tides (*Figure 2.6*). Tidal barrages plants are fundamentally composed by a dam structure with sluice gates to control the flow of the seawater. The sluice gates remain closed at high tide to hold the water level inside the dam at its highest. When the tide recedes, a difference in water level in between the seaward and the inward of the dam is created. The potential energy from the water level difference can then drive low-head hydro turbines to generate electricity. There are a variety of turbine designs and they can be designed to operate in both directions, ebb and flood.

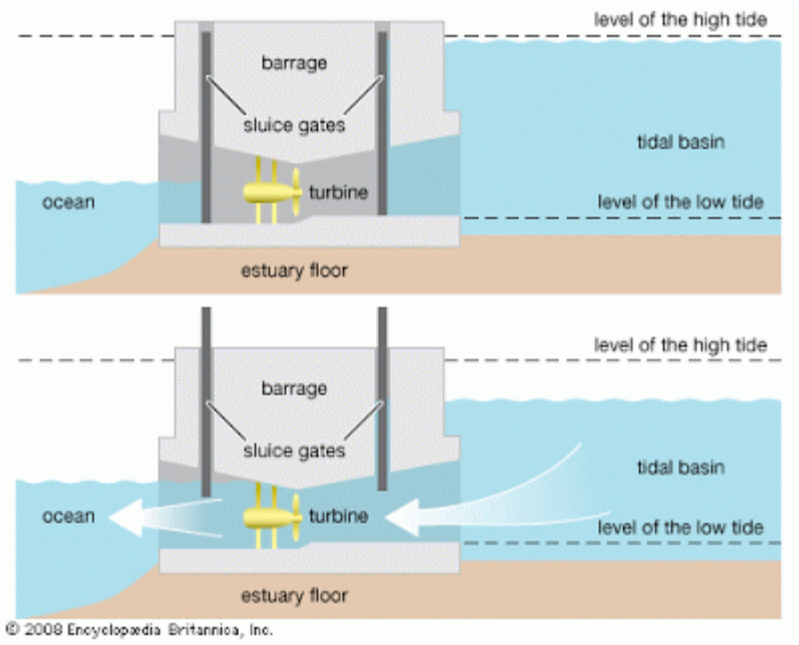

Figure 2.6: Tidal barrage operation. Source: [26]

Tidal range is considered a mature technology, is reliable and has excellent potential. However the current issues restricting its development are the high civil infrastructure costs, the worldwide shortage of viable sites and the environmental impact. The construction of a tidal barrage requires a vast quantity of materials to withstand huge loads produced from the dammed water. Besides that, to achieve economic viability, this kind of projects must be very large which consequently entails unacceptable environmental impacts.

2.3.2. Tidal current systems

Tidal current systems extract the kinetic energy of the moving water in a similar way to windmills extract energy from air. Installation of tidal current devices requires minimum

land use. In contrast to tidal barrages, where an artificial hydraulic head is created using dams or penstocks, tidal hydrokinetic converters are constructed without significantly altering the natural path of the water stream. Tidal current devices are normally fully submerged, therefore they will not affect optically or acoustically their surroundings (*Figure 2.7*). These technologies can be arranged in multi-unit array tidal farms. Modularity and scalability are attractive features of this technology.

Figure 2.7: Fully submerged tidal current devices. Source: [27]

Tidal current technology is still in its infancy. However, recent developments facilitate prospects for commercial deployment of some schemes in the near future. This system is gaining in popularity due to the lower cost and environmental impact compared to tidal barrages.

2.4. Tidal current power: energy extraction

Tidal currents are a form of kinetic energy and its basic physical principles for extracting energy are virtually similar to those for wind. The kinetic energy of a moving fluid can be extracted by a turbine rotor. Therefore, the analysis of wind turbines can be extended for tidal current turbines. However, there are several differences in operating conditions. Water is approximately 800 times denser than air. Power extraction is proportional to the fluid density and to the cross-sectional area of the rotor of the turbine; as a result, power extracted by tidal current turbines will be substantially higher than that produced by wind turbines when similar flow speeds are considered. In consequence, smaller and hence more manageable devices can be installed as it is shown in *Figure 2.8*.

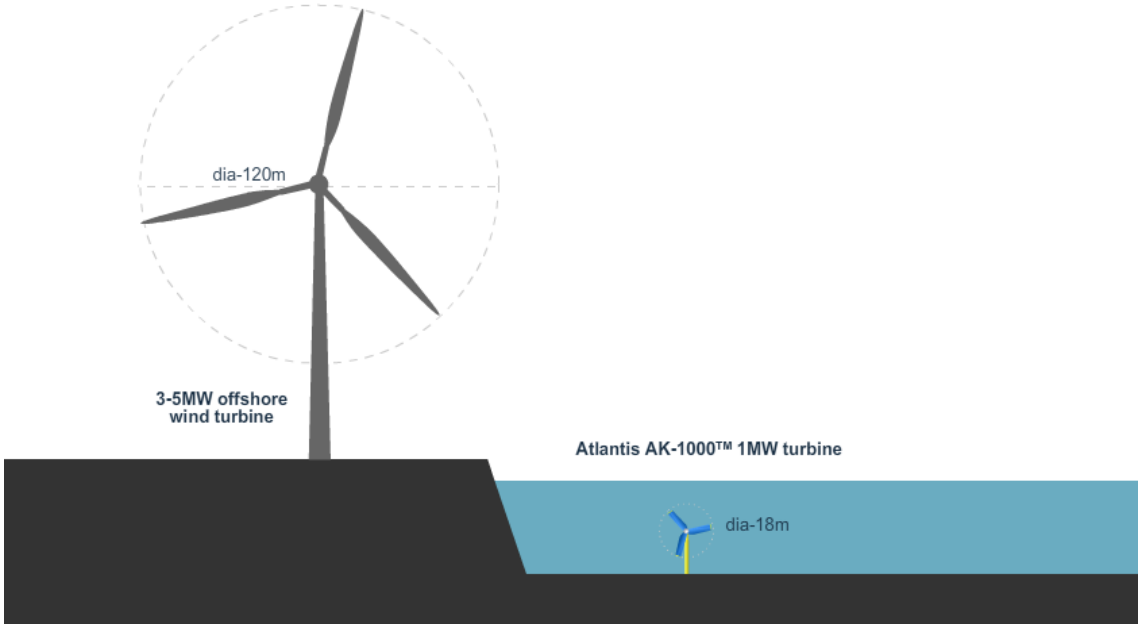

Figure 2.8: Technology comparison: wind turbine (left) vs. tidal current turbine (right). Source:[11]

In contrast to atmospheric air flows, the availability of tidal currents can be accurately forecasted for many years into the future, facilitating network balancing. Another specific advantage of tidal current devices is its limited environmental impact, as generating electricity from the tides creates no greenhouse gas emissions or water pollutants. Tidal power devices are fully or nearly completely submerged in water well offshore and their installation requires minimum land use, thus minimum visual and acoustic impact is guaranteed. Finally, submerged marine current converters are considered to operate in safe environment, disturbances caused by extreme weather conditions are significantly attenuated to the depths of 20 - 30 m, where devices will be generally placed. However, since tidal current turbines operate in water, there are some rather difficult problems associated with installations, survivability and maintenance which need to be solved to achieve commercial stage of exploitation. Tidal current devices will encounter larger forces than wind turbines; mostly bending forces due to lift rather than the gravity and centrifugal forces that dominate for a wind turbine rotor. Its design presents structural challenges and will need to take into account the overall thrust from the kinetic energy of the flowing water. Furthermore, tidal current turbines must be able to generate during both, flood and ebb currents, and be able to withstand the structural loads when not generating electricity.

At the present time the costs of tidal current technology are extremely high and they will decrease as the technology advances [28]. The current issues restricting the developments of tidal current turbines are installation challenges, maintenance, electricity transmission, loading conditions and environmental impacts. Improvements in these matters will enhance the viability of these projects and they will become feasible and reliable.

2.5. Tidal technology: tidal current energy conversion devices

Tidal current energy offers a great deal of promise, especially during the early stages when the highest-energy sites are all still available for the implementation of new systems. The technology is designed to harness the kinetic energy of the fast flowing water in tidal areas. A huge number of devices are at the research and development stages and only a minority have reached the pre-commercial stage. The industry is growing rapidly and the hydrokinetic energy technology is one of the newest and fastest growing sectors of renewable energies [29]. Research and development in this emerging field have led to the design of several types of device to capture this energy.

2.5.1. Horizontal axis turbine

Horizontal axis turbines are the most common mean of extracting power from marine currents and are rather similar in design to wind turbines. Although there are a variety of approaches, including ducts, variable pitch blades and rim generators, all of these devices consist of a turbine with a horizontal axis of rotation, aligned parallel to the current flow. These axial flow turbines generally use a power take-off mechanism involving a generator coupled to the shaft of the turbine, either directly or via a gearbox, to produce electricity.

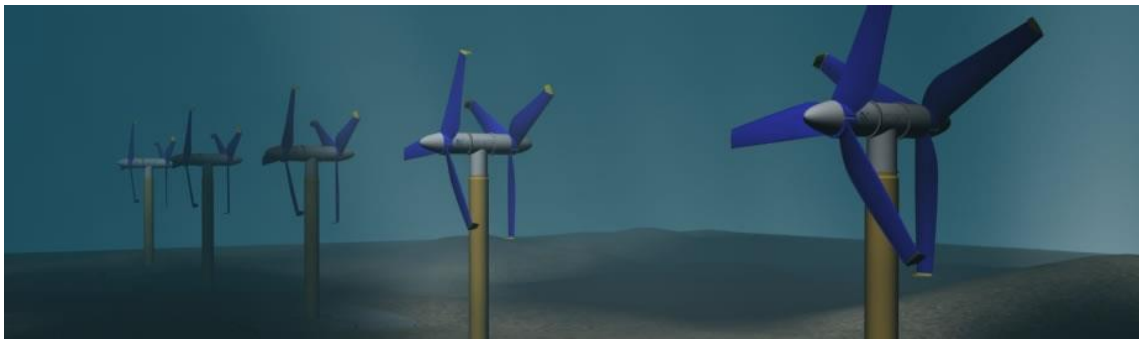

Figure 2.9: Horizontal axis turbines conceptual representation. Source: [11]

The horizontal axis turbines are further split into two categories: Non-ducted (*Figure 2.9*) and ducted (*Figure 2.10*). Ducts are fixed structures placed around the outside of a rotor to increase its power creating a funnel effect which increases the flow rate through the rotor.

.

Figure 2.10: Ducted horizontal axis turbine (Alstom/Clean-Current)

Horizontal axis tidal turbines are the most developed tidal current energy extraction devices. Further section 2.5.6 comprises a compilation of the most important horizontal tidal turbine developers.

2.5.2. Vertical axis turbine

Vertical axis turbines extract energy from the tides in a similar manner to horizontal ones; however the turbine is mounted on a vertical axis. The tidal stream causes the rotors to rotate around the vertical axis and generate power. They are also called cross flow turbines since the direction of flow is across the axis of rotation. There are several different designs in use, with some incorporating variable pitch blades (either controlled or freely moving) or shaped ducts to direct or restrict fluid flows. Examples of vertical axis turbines can be seen in *Figure 2.11*.

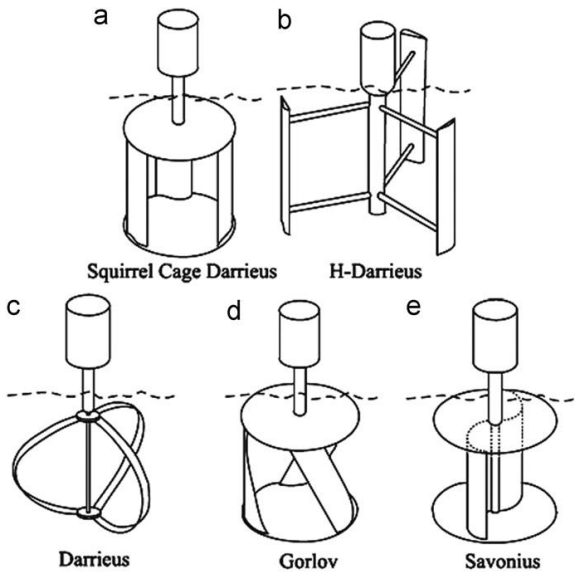

Figure 2.11: Different designs of vertical axis tidal turbines

2.5.3. Oscillating hydrofoil

Oscillating systems use the force of lift generated by an oscillating wing whose incidence is controlled by an appropriate system. When tidal flow passes over it, under the effect of the lift, the wing moves perpendicularly to the flow (*Figure 2.12*). Up to a certain degree of incidence, the angle of incidence is actively reversed by an appropriate system; the lift is then orientated in the opposite direction, reversing the motion of the wing. This movement is reproduced cyclically. The oscillating motion drives fluid in a hydraulic system to be converted into electricity.

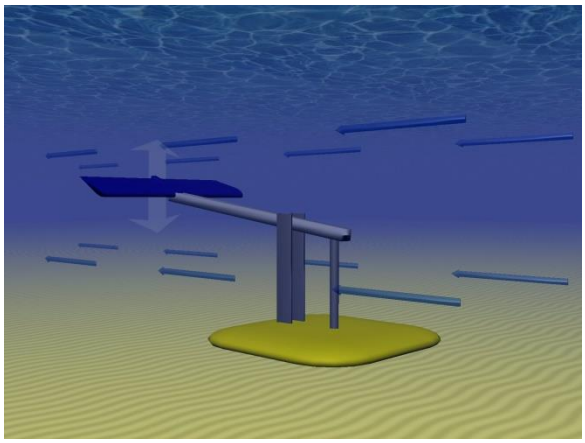

Figure 2.12: Oscillating hydrofoil conceptual representation. Source: [30]

2.5.4. Other designs

This covers those devices less common and developed. An example of them is the Archimedes screw, which is a helical corkscrew-shaped device that draws power from the tidal stream as the water moves up and through the spiral turning the turbines (*Figure 2.13*). Another special design that is worth mentioning is the Tidal kite, which consists of a kite tethered to the sea bed carrying a turbine below the wing. The kite flies in the tidal stream, swooping in a figure-of-eight shape to increase the speed of the water flowing through the turbine (*Figure 2.13*).

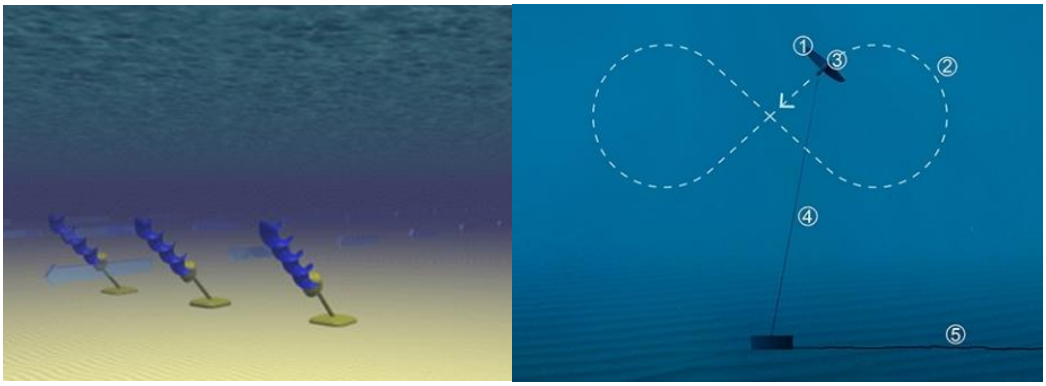

Figure 2.13: Archimedes tidal screw (left) and tidal kite (right)

2.5.5. Methods to fix the devices the seabed

Tidal converters are mounted to a support structure that is required to withstand the harsh environmental conditions. The choice of the foundation depends mainly on geographical conditions such as water depth, seabed conditions, streams etc. and the type of device to be installed. In addition to the categories of devices identified above, there is also a range of methods to fix the converter to the seabed.

There are three main support structures. The first one, seabed mounted gravity base, consists on a big mass of concrete and steel, which is attached to the base of the structure to provide stability. The second option, pile mounted, which is pinned to the seafloor using one or more steel or concrete beams. And finally, the third option is the floating foundation; its structure is usually moored to the seafloor using chains or wire. In this case, the device is fixed to a downward pointing vertical beam, which is fixed to a floating structure.

2.5.6. Compilation of the most important horizontal tidal turbine developers

Horizontal tidal turbines are the most developed design within the field of tidal energy extraction. Therefore the following table presents a collection of some of the most important horizontal tidal turbine developers and their most known device designs.

2. Background on tidal energy

Company	Device	Location	Technic features												Rated Power	Production capacity	Status	Illustration
			Type	Water depth	Distance from the shoreline	Diameter	nº blades	Cut-in speed	Rated speed	Operation hours	Structure	Installation	Connection to the grid	More features				
Marine Current Turbine Ltd.	SeaFlow	Lynmouth, Devon (UK)	Twin horizontal axis rotors	20-30 m	<1 km	11 m	2		2-3 m/s		Mounted on a pile tower drilled into the sea bed	Carried out from the jack up barge, diverless	No, too expensive for just one turbine	Blades can be pitched through 180º	300 kW		Installed in summer 2003	
	SeaGen (S)	Strangford Lough, Northern Ireland (UK)	As above	24-40 m	400 m	16-20 m	2	0,7-1 m/s	>2,4 m/s	18-20 h/day	As above	As above	Yes	The world's first commercial-scale tidal turbine.	1,2-2 MW	7,8 GWh/y	Installed in May 2008	
	SeaGen (U)	FORCE Bay of Fundy (Canada)	3 horizontal axis rotors	22-50 m		16-20 m	2	0,7-1 m/s	>2,4 m/s		Structure pivoted on the seabed			As above	1,8-3 MW	12,3 GWh/y	The device is currently at design stage	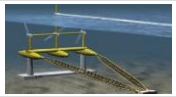
Andritz Hydro Hammerfest	Tidal Stream Turbine HS300	Kvalsund (Norway)	Horizontal axis rotor	Deep water 50 m		20 m	3	1 m/s	1,7 m/s	>16000 h production track record	Turbines deployed on the seabed, fixed by gravity, pins or pilings	Installation is diverless with only the support of standard ROVs and moored barges	Yes	Variable pitch, yawing system, variable speed	300 kW	>600 MWh/y	Installation in 2003, connection to the grid in 2004	
	Tidal Stream Turbine HS1000	EMEC Orkney Islands, Scotland (UK)	As above	Deep water 35-80 m (52 m)		21 m	3	1 m/s	2,7 m/s		As above	As above	Yes	As above	1000 kW	>3,1 GWh/y	Installed in December 2011, connected in 2012	
Magallanes renovables	Magallanes Project Trimarán	EMEC Orkney Islands, Scotland (UK)	Twin horizontal contra-rotating axis rotors				3		>1,5 m/s		High-stability floating platform	Low cost installation	Yes	Variable blade pitching. The first Spanish project on tidal currents	2 MW	86 GWh/y	Development of a 1:10 scale model in 2013, planning the 1:1 for 2015	
OpenHydro Ltd.	Open Centred Turbine	EMEC Orkney Islands, Scotland (UK)	Open centred horizontal axis rotor			6 m	Multiblade				Seabed mounted gravity base	The test rig allows for the turbine to be raised out of the water easily	Yes, but from 2008		250 kW		Testing in 2006	
	Open Centred Turbine (commercial)	FORCE Bay of Fundy (Canada)	Open centred horizontal axis rotor			10 m	Multiblade				As above	Simplified design. Low manufacture cost	Yes	First large-scale device in North America	1 MW		Installed in November 2009	
	Open Centred Turbine (commercial array)	As above	Open centred horizontal axis rotor			6 m	Multiblade				As above	As above	Yes	2 turbines array	2x2MW=4MW		Planned installation in 2015	

Table 2.1: Horizontal tidal turbine developers I

2. Background on tidal energy

Company	Device	Location	Technic features												Rated Power	Production capacity	Status	Illustration
			Type	Water depth	Distance from the shoreline	Diameter	nº blades	Cut-in speed	Rated speed	Operation hours	Structure	Installation	Connection to the grid	More features				
Atlantis Resources Corp Ltd.	AR1000	EMEC Orkney Islands, Scotland (UK)	Horizontal axis rotor	Deep water >25 m		18 m	3		>2,65 m/s		Gravity based structure	DP2 vessels	Yes		1 MW		Testing in summer 2011	
	Nereus I Nereus II (AN Series)	San Remo (Australia)	Horizontal axis rotor + Aquafoils (capture momentum to drive a chain)	Shallow water <25 m		12 m x 4 m	Multi Aquafoils				Mounted on a pile tower drilled into the sea bed	Carried out from the jack up barge, diverless	Yes	The turbine is robust and can withstand water flow containing significant debris	150 kW 400 kW		Tow testing in July 2008	
	Selon (AS Series)	San Remo (Australia)	Ducted horizontal axis turbine	Deep water >25 m		16 m	Multi bidirectional blades		3 m/s		Gravity based structure	DP2 vessels	Yes		500 kW		Tow testing in August 2008	
Lunar Energy Ltd.	Lunar tidal turbine (LTT, also Rotech Tidal Turbine)	EMEC Orkney Islands, Scotland (UK)	Ducted (Venturi) bidirectional horizontal axis turbine	Very deep water from 25 to >40 m		rotor: 16 m ducted: 21 m	Multi bidirectional blades		3 m/s		Gravity 3 leg foundation, moduled components	Moored barges, rapid deployment with minimal seabed preparation. Easy maintenance (on land)	Yes	Simple & robust design. Hydraulic motor and generator. No need to pitch of the blades	1 MW		Testing in 2007	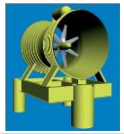
Verdant Power, Inc	Kinetic Hydropower System (KHPS, also Gen4 and Gen5)	RITE Project East River, New York (USA)	Horizontal axis rotor			5 m	3 blades	1 m/s	2,1 m/s	9000 h	Gravity based structure	Moored barges, operation & maintenance costs optimized	Yes	Blades can be pitched through 180º. Designed to works in arrays	35 kW	70 MWh/y	Testing September 2012	
Alstom	Tidal stream turbine (TGL turbine)	EMEC Orkney Islands, Scotland (UK)	Horizontal axis rotor	>25 m		18 m	3 blades	1 m/s	2,7 m/s		Buoyant turbine deployed on its seabed support structure (fixed by gravity)	No divers or vessel needs. It uses a patented system to winch the buoyant nacelle on the seabed	Yes	Variable pitch, yawing nacelle. The turbine can be installed & uninstalled rapidly	1 MW		Currently testing (2013-14)	
Clean Current Power Systems Inc.	CC035A CC050A CC075A	FORCE Bay of Fundy (Canada)	Ducted horizontal axis turbine	>7 m >10 m >15 m		3,5 m 5 m 7,5 m	Multi bidirectional blades	0,7 m/s	3 m/s		Can be either seabed mounted or mounted to a floating structure	Easily deployed and retrieved, even in remote locations	Yes	Simple, robust design. Bearing yawing system. Minimum maintenance during 25 years	65 kW 130 kW 295 kW		Currently testing (finishing target at spring 2015)	
Straum	Hydra Tidal	MORILD II Gimsoy stream in Lofoten (Norway)	4 horizontal axis rotor	water depth independent			2 blades				Patented floating design that can be anchored at different depths	Easy remote operation, towing, docking, installation, as well as easy access for low cost O&M	Yes	Wooden turbine blades that can be pitched 180 degrees to utilize energy in both directions	1 ,5 MW		Testing from November 2010 till November 2012. Currently out of service	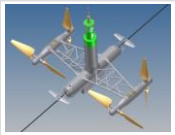
Ocean Dynamic Power	Lyken water turbine	(Sweden)	Horizontal axis turbine (without propeller)				6 blades, without propeller, the whole turbine rotates				Patented floating design anchored to the seabed	Cheap & easy installation. Light enough to be lifted onto support vessels. Low O&M cost	Yes	Produces 20% more energy than a wind turbine for the same investment			In the process of creating the first full-scale Lyken systems	

Table 2.2: Horizontal tidal turbine developers II

Chapter III

Area of study

3.1. Geographical location

The Ría de Vigo, the southernmost of the Rías Baixas, in Galicia, north-west of Spain, is located approximately between 42º09'-42º21'N and 8º36'-8º54'W.

Its basin is a rift valley formed by two geological faults that are aligned from North to South and correspondingly from Northeast to Southwest.

The Ría stretches along approximately 32 km and covers an area of 185 km^2 with an external width of about 10 km and a depth of about 26 m in its central part. It has a volume capacity slightly over 3000 km^3. ´

The ratio surface/volume is 0.05 m^{-1}, typical from the V shaped estuaries, which gradually expand and become deeper towards the mouth. In its innermost part, this quotient is 0.40 m^{-1}, more akin to a typical estuary system. Morphologically, its cross section is defined by a deeper central channel that rises quickly to the banks with a slope higher than 4º.

Figure 3.1: Area of study

The plan of the estuary (*Figure 3.1*) portrays two different parts: the San Simón Bay and the rest of the estuary. The first one is located at the bottom of the estuary and consists of a wide basin, which is almost completely silted with sediments. Up to 60% of its surface is exposed (dry) during low tide. The second part is attached to the first one through the Rande Strait, which is around 700 m wide, from which the estuary regularly widens towards the mouth. This part can be subdivided in two areas; a medium area of approximately 15 km length, between the strait (depths of 20 m) and the line joining Borneira Tip with Mar Cape (depths of 40 m), and an outer area from this line to Cíes Islands.

The Cíes Islands connect the Atlantic Ocean with the estuary and divide the mouth of the river into two main mouths of very different physical and hydrodynamic characteristics; the northern mouth, with a maximum depth of 23 m (*Figure 3.2*) and a width around 2.5 km, and the southern mouth, with greater maximum depth (52 m) and width (5 km). Furthermore, between the two islands there is a small entrance of 7.5 m depth approximately.

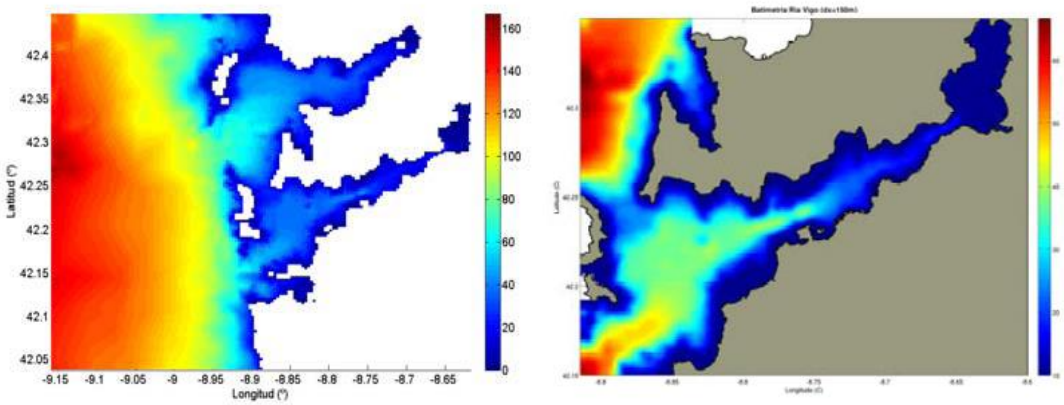

Figure 3.2: Bathymetry of the Ría de Vigo

Circulation patterns within the estuaries are strongly conditioned by the mesomareal and semidiurnal tides, with an average tidal range of about 3 m, and also by other factors including wind regime on the continental platform, wind regime within the estuary itself, river discharge, air temperature and frequent episodes of upwelling that have great influence on the residual circulation (mainly in summer).

The Ría de Vigo will behave as an estuary at its fullest in winter, when the contribution of freshwater from the river is large enough. During the summer months it may only be considered strictly the innermost part of the estuary [31].

3.2. Meteo-oceanographic description

As previously mentioned, the Ría de Vigo depicts three different areas. The outermost area, between Cíes Islands and the line joining Mar Cape and Borneira Tip, has hydrodynamic features characterised mainly by tides and continental wind. In the innermost area, San Simon Bay, circulation is due to tidal combination, local wind and

freshwater inputs from the mouth of the Oitabén-Verdugo system. The central area circulation is under the influence of all the aforementioned mechanisms.

The main meteorological and oceanographic variables describing the area of study are the following:

i) Wind

The coastal winds, over the continental shelf, show clear seasonal patterns. During spring and summer, the prevailing wind comes from the N-NE, while during the remainder of the year S-SW winds predominate. The annual average intensity is lower than 5 m/s, with mean monthly values that eventually may reach 10 m/s.

In the inner part of the estuary, the wind is essentially influenced by the topography. Throughout the year, the prevailing wind tends to blow along the axis of the estuary, channelled through the nearby mountains. In winter, the wind flow velocities may occasionally reach 10 m/s, albeit the annual average intensity does not exceed 5 m/s. During summer, the daily wind variation follows a sea-breeze pattern.

ii) Air temperature

Air temperature in the estuary oscillates between a mean value of 11.5ºC in winter and 19.3ºC in summer, following a typical pattern characterised by low temperatures in winter and high temperatures in summer. Air temperature variations significantly influence the temperature of the uppermost layers of the water.

iii) Hydrography

The main source of continental water in the sea loch is the system formed by the Verdugo and Oitabén rivers. However, the total flow rate supplied by this system is lower than 10 m^3/s during 75% of the time, and lower than 30 m^3/s in 92 - 96% of the time. This is reflected in the composition of the estuary surface water, which consists of 95% of oceanic water, and the remaining 5% of continental water.

iv) Temperature and water salinity

The water temperature is usually between 13 -18ºC. The temperature at the surface of the water column is tightly regulated by seasonal air temperature cycles. Temperature inversion occurs in the estuary between November and March, when the water in the deeper layers is approximately 1ºC hotter than at the surface. Therefore, the salinity fluctuates between 33.3 and 35.7 depending on the depth, position within the estuary, and time of the year. Salinity values are usually minimum in winter and maximum in summer. Throughout the estuary the thermohaline distribution is strongly influenced by coastal winds that determine episodes of cooler and saltier water inputs through the deeper layers of the water column.

v) Sea level

The sea level in the Ría de Vigo has an important astronomical tidal component of semidiurnal character, and a less relevant component associated to atmospheric pressure gradients (meteorological tide).

The astronomical tide presents a range between 0.82 m and 4.21 m, with a mean value of 2.4 m. Neither the amplitude nor the phase of the tidal wave varies significantly along the estuary, at least downstream Rande Strait.

The meteorological tide is generally much less relevant than the astronomical, presenting an average level close to zero. Notwithstanding, the meteorological tide can be comparable to the astronomical tide (sometimes) by the minimum and maximum peaks observed, -1.08 m and 0.69 m, respectively, for the 1992 - 2009 period.

vi) Waves

Due to a lack of data sets measured inside the estuary, the information presented has been compiled from the reports of Puertos del Estado on the observations made in the Silleiro buoy in 2006 and 2007 (*Figure 3.3*). The characterization of the typical wave regime will be incomplete because the shelter provided by the Cíes Islands (and therefore the lower intensity of wind inside the estuary compared with coastal breezes), which makes the wave regime within the estuary significantly different from the existing regime in external waters. However, data from the Cape Silleiro buoy do allow extracting information of interest.

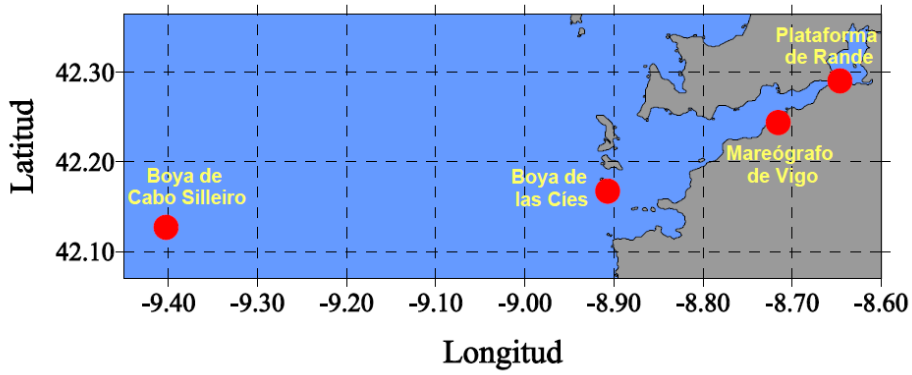

Figure 3.3: Measurement stations from Puertos del Estado and MeteoGalicia-Intecmar in the vicinity of the Ría de Vigo

The annual averages of the wave parameters show that the average significant wave height for both years is around 2.40 m, and between 41% and 43% of the data are among Hs = 1 and 2 m. Peak periods follow a Gaussian distribution centred at 10.08 s (33% -38%), but tend to be slightly smaller in summer. The predominant wave direction is between 270° (W) and 360° (N), with a frequency in the two years analysed above 70%, and practically independent of the season. In 2006, there was a slightly higher dispersion of wave data during the spring and autumn, while a greater dispersion was observed in 2007 during the summer.

Throughout the year, the most energetic waves are observed during the winter months, with maximum values of H_s 8.33 m (2006) and 10.38 m (2007), and average values of H_s that practically double summer values. The most energetic seasons are winter and spring, with over 57% of significant wave height higher than 2 m. Autumn is also very energetic, similar to spring. By contrast, summer is not very energetic, with only approximately 15% of significant wave height higher than 2 m.

From these data it can be gathered that the majority of waves are of swell type (generated elsewhere and spread to the point of observation, with periods longer than 4 seconds), while waves generated by local winds (called sea type, with shorter periods) are not very common.

vii) Water quality

The quality of the estuary's water is affected by the ability to renew the water and pollutant inputs. Among these, it is worth highlighting the contribution from aquaculture (essentially mariculture) and activities related to the presence of the port. While in general pollution levels found are relatively low in specific areas, such as San Simón Bay (low water renewal rates) or the port environment, high concentrations of heavy metals or organic contamination may also be present. Also noteworthy is the existence of several discharges of wastewater into the estuary by submarine emissaries, although reliable information about their features has not been obtained.

viii) Currents

Currents across the sea loch are determined primarily by tides, as could be expected in an estuary with these features, even though local wind and freshwater discharges may also have a secondary role, especially in the upper layers.

In relation with the sampling area and the season, the analysis of the results from different field campaigns shows mean celerity values in the surface layer ranging between 0.3 m/s and 0.8 m/s, and currents higher than 1.25 m/s at some points. In the deep layer, celerities are much less intense, ranging from 0.06 m/s to 0.15 m/s, with peaks of up to 0.8 m/s. In general, the magnitude and direction of the currents depend on the depth and the width of the river at the point of measurement. Close to the surface, the wind has a relatively important influence and justifies up to 94% of streams variability, while it loses importance in the deepest layers, where the most important driver is the tide [32].

Chapter IV

Data and Methods

Modelled data were used to evaluate the resource. The simulation of Ria de Vigo tidal stream was carried out implementing the ROMS modelling system, which generated the distribution of the tidal current velocities within the estuary allowing to obtain the tidal power potential of the study area. To verify the suitability of the modelled data, the numerical model was calibrated by comparing model data with field campaign measurements conducted in the area of application.

4.1. Numerical model: ROMS

The approach to tidal stream resource assessment followed in this study of the Ría de Vigo was to use a numerical model of tidal flows around the estuary. The aim of this was that, when properly calibrated and validated, at a high enough resolution and run for a long enough period, the model could predict with enough accuracy the variation of the tidal stream in both time and space. The simulation of the tidal stream at the Ría de Vigo was carried out using the ROMS modelling system.

The Regional Ocean Modelling System (ROMS), developed in the UCLA (University of California, Los Angeles), is a three-dimensional, free-surface, terrain-following numerical model that solves three dimensional Reynolds-averaged Navier-Stokes equations using the hydrostatic and Boussinesq assumptions [33]. ROMS uses the Arakawa-C differencing scheme to discretise the horizontal grid in curvilinear orthogonal coordinates, and finite difference approximations on vertical stretched terrain-following coordinates (sigma) [34].

It is a split-explicit model that solves separately the evolution of the free surface and the equations of vertically integrated momentum (2DH), using a short computational time step, on one hand, and the equations of temperature, salinity and 3D momentum (baroclinic terms) on the other, with a longer computational time step. This reduces considerably the duration of the numerical simulations without having any appreciable effect on the validity of the obtained solutions [35].

For this research, ROMS_AGRIF version has been applied. The AGRIF subversion, developed in the IRD (Institut de Recherche pour le Developpement), includes advanced processes of adaptive mesh refinement [36][37] and a set of pre- and post-processing data routines, that facilitates the preparation of the necessary files for the configuration of each simulation, as well as, the analysis and representation of the final results.

The ROMS model or variant ROMS_AGRIF has been successfully applied in a variety of different scenarios, both large spatial scales and smaller scales [38][39][40].

4.1.1. Equations of motion

The primitive equations in Cartesian coordinates are shown here. The momentum balance in the *x* and *y* directions are [41]:

$$\frac{\partial u}{\partial t} + \vec{v} \cdot \nabla u - fv = -\frac{\partial \phi}{\partial x} - \frac{\partial}{\partial z}\left(\overline{u'w'} - \nu \frac{\partial u}{\partial z}\right) + \mathcal{F}_u + \mathcal{D}_u \tag{4.1}$$

$$\frac{\partial v}{\partial t} + \vec{v} \cdot \nabla v + fu = -\frac{\partial \phi}{\partial y} - \frac{\partial}{\partial z}\left(\overline{v'w'} - \nu \frac{\partial v}{\partial z}\right) + \mathcal{F}_v + \mathcal{D}_v \tag{4.2}$$

The time evolution of a scalar concentration field, *C(x,y,z,t)* (e.g. salinity, temperature, or nutrients), is governed by the advective-diffusive equation:

$$\frac{\partial C}{\partial t} + \vec{v} \cdot \nabla C = -\frac{\partial}{\partial z}\left(\overline{C'w'} - \nu_\theta \frac{\partial C}{\partial z}\right) + \mathcal{F}_C + \mathcal{D}_C \tag{4.3}$$

The equation of state is given by:

$$\rho = \rho(T, S, P) \tag{4.4}$$

In the Boussinesq approximation, density variations are neglected in the momentum equations except in their contribution to the buoyancy force in the vertical momentum equation. Under the hydrostatic approximation, it is further assumed that the vertical pressure gradient balances the buoyancy force:

$$\frac{\partial \phi}{\partial z} = -\frac{\rho g}{\rho_o} \tag{4.5}$$

The final equation expresses the continuity equation for an incompressible fluid:

$$\frac{\partial u}{\partial x} + \frac{\partial v}{\partial y} + \frac{\partial w}{\partial z} = 0 \tag{4.6}$$

For the moment, the effects of forcing and horizontal dissipation will be represented by the schematic terms $\mathcal{F}$ and $\mathcal{D}$, respectively. The variables used are shown here:

$\mathcal{D}_u, \mathcal{D}_v, \mathcal{D}_C$	diffusive terms
$\mathcal{F}_u, \mathcal{F}_v, \mathcal{F}_C$	forcing terms
$f(x, y)$	Coriolis parameter
g	acceleration of gravity
$h(x, y)$	bottom depth
ν, ν_θ	molecular viscosity and diffusivity
K_m, K_C	vertical eddy viscosity and diffusivity
P	total pressure $P \approx - \rho_o g z$
$\phi(x, y, z, t)$	dynamic pressure $\phi = (P/\rho_o)$
$\rho_o + \rho(x, y, z, t)$	total *in situ* density
$S(x, y, z, t)$	salinity
t	time
$T(x, y, z, t)$	potential temperature
u, v, w	the (x,y,z) components of vector velocity $\vec{v}$
x, y	horizontal coordinates
z	vertical coordinate
$\zeta(x, y, t)$	the surface elevation

These equations are closed by parameterizing the Reynolds stresses and turbulent tracer fluxes as:

$$\overline{u'w'} = -K_M \frac{\partial u}{\partial z}; \qquad \overline{v'w'} = -K_M \frac{\partial v}{\partial z}; \qquad \overline{C'w'} = -K_C \frac{\partial C}{\partial z}. \tag{4.7}$$

An overbar represents a time average and a prime represents a fluctuation about the mean.

Vertical boundary conditions

The vertical boundary conditions can be prescribed as follows:

top $\left(z = \zeta(x, y, t)\right)$:

$$\begin{aligned} K_m \frac{\partial u}{\partial z} &= \tau_s^x(x, y, t) \\ K_m \frac{\partial v}{\partial z} &= \tau_s^y(x, y, t) \\ K_C \frac{\partial C}{\partial z} &= \frac{Q_C}{\rho_o c_P} \\ w &= \frac{\partial \zeta}{\partial t} \end{aligned} \tag{4.8}$$

and bottom ($z = -h(x, y)$):

$$
\begin{aligned}
K_m \frac{\partial u}{\partial z} &= \tau_b^x(x,y,t) \\
K_m \frac{\partial v}{\partial z} &= \tau_b^y(x,y,t) \\
K_C \frac{\partial C}{\partial z} &= 0 \\
-w + \vec{v} \cdot \nabla h &= 0
\end{aligned}
\tag{4.9}
$$

The new variables above are:

Variable	Description
Q_C	surface concentration flux
τ_s^x, τ_s^y	surface wind stress
τ_b^x, τ_b^y	bottom stress

The surface boundary condition variables are defined in the table above. Since Q_C is a strong function of the surface temperature, we usually choose to compute Q_C using the surface temperature and the atmospheric fields in an atmospheric bulk flux parameterization. This bulk flux routine also computes the wind stress from the winds.

On the variable bottom, $z = -h(x,y)$, the horizontal velocity components are constrained to accommodate a prescribed bottom stress which is a choice of linear, quadratic, or a log layer, depending on the options. The vertical scalar concentration fluxes may also be prescribed at the bottom, although they are usually set to zero.

Horizontal boundary conditions

As distributed, the model can easily be configured for a periodic channel, a doubly periodic domain, or a closed basin. Code is also included for open boundaries which may or may not work for your particular application. Appropriate boundary conditions are provided for u, v, C and ς.

The model domain is logically rectangular, but it is possible to mask out land areas on the boundary and in the interior. Boundary conditions on these masked regions are straightforward, with a choice of no-slip or free-slip walls.

If biharmonic friction is used, a higher order boundary condition must also be provided. The model currently has this built into the code where the biharmonic terms are calculated. The high order boundary conditions used for u are $\frac{\partial}{\partial x}\left(\frac{h\nu}{mn}\frac{\partial^2 u}{\partial x^2}\right) = 0$ on the eastern and western boundaries and $\frac{\partial}{\partial y}\left(\frac{h\nu}{mn}\frac{\partial^2 u}{\partial y^2}\right) = 0$ on the northern and southern boundaries. The boundary conditions for v and C are similar. These boundary conditions were chosen because they preserve the property of no gain or loss of volume-integrated momentum or scalar concentration.

4.1.2. Case study in Ría de Vigo

The finite difference mesh is a Cartesian grid covering the estuary and its surroundings. The horizontal grid size is 150 x 150 m and has ten sigma levels on the vertical. The vertical discretization has been done in order to have enough resolution on both surface and bottom layers according to the computational limitation of an operational system. However, in this case the Ría de Vigo, as in many other similar assessments and for the sake of simplicity, it has been deemed unnecessary to take into account the sigma levels because tidal currents usually have a reasonably uniform vertical distribution. Therefore, the 3D numerical model has been used as a vertically averaged 2DH model. The horizontal domain of the model has been divided into 176 x 153 = 26,928 grid points. In this study, for simplicity and considering that only tidal currents are of interest, water density has been assumed to be homogeneous with a value of 1025 kg/m^3. Density-driven effects have been consequently omitted. The external and internal time-steps used to run the simulation are 18 s and 2 s respectively. The simulation has been run for an entire tidal cycle of 28 days. The output time step is one hour.

4.1.3. Numerical model calibration

The first step in the practical application of any numerical model is its calibration by comparing the prognostic variables with field data. For hydrodynamic models, the usual procedure is to compare data series of sea level and current velocity at various depths to ensure that the model is able to represent the temporal evolution of these parameters.

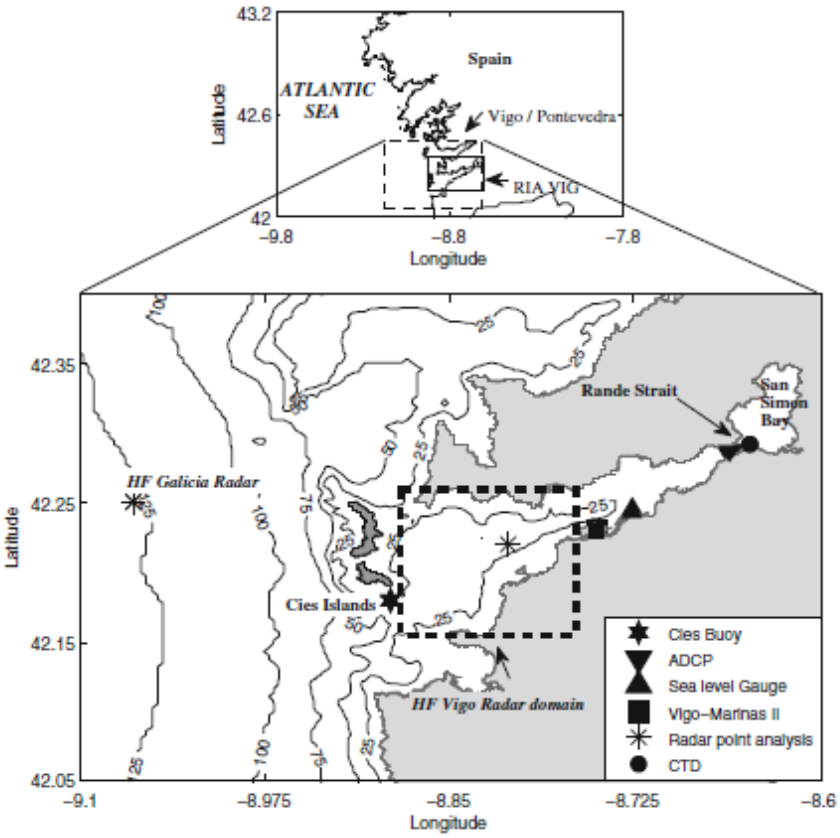

Figure 4.1: Measuring points for surface currents, sea level, meteorological parameters (Cíes buoy and temperature/salinity profiles. Source: [42]

Data from different measuring devices were used to validate the model [42]: Sea-level evolution was measured at the Vigo harbour tide gauge (MIROS Radar, www.puertos.es). Surface velocities were compared with high-frequency radar (HF-RADAR) and Horizontal Acoustic Doppler Current Profiler (HADCP) data. The HF-RADAR (University of VIGO, http://eddy.uvigo.es/) was placed in the centre of the Ría and provided 250 m resolution hourly data. The HADCP (MeteoGalicia) was located in Rande Strait. Conductivity, temperature, and depth profiles (CDT) were used to validate simulated temperature and salinity. CTD profiles were surveyed by INTECMAR (www.intecmar.org) in the Rande Strait twice a week. Finally, wind data were obtained from one oceanographic buoy (Cíes buoy) and one meteorological station (Vigo-Marinas II). All these locations are shown in *Figure 4.1*.

With the aim of validating the model, three simulation periods of 15 days were compared with measured data. These periods were selected after taking into account the available hydrodynamic and atmospheric data for the validation (summary on *Table 4.1*). Period 1 (P1) showed typical wet season conditions with precipitation and high river discharge (>30 m^3/s). From 12th to 20th November, strong northward winds blew along the shelf and were followed by a change in wind direction, formed by weaker southward winds. Periods 2 (P2) and 3 (P3) were both in April 2011 and showed springtime characteristics, with higher solar radiation values and less precipitation and river discharge (around 10 m^3/s). The strongest winds in both periods were from the

north (from 10th to 13th for P2 and 23rd to 29th for P3), with high direction variability over the rest of the periods.

Configuration	Period	Data available
P1	12-30 November 2010	HADCP, CTD, tide gauge
P2	2-15 April 2011	HF-RADAR, CTD, tide gauge
P3	17 April – 1 May 2011	HF-RADAR, CTD, tide gauge

Table 4.1: Configuration, periods and data used to validate the model

Sea-level time series results revealed low errors and correlation values up to 0.9. On the other hand, surface velocities showed acceptable results on the radar area, where tidal and wind circulation patterns were well reproduced by the model. Analysis of scattered data revealed correlation values close to 0.8 for the eastward component and 0.7 for the northward component (*Figure 4.2*).

Regarding the HADCP data, after comparison, modelled data tended to overestimate ingoing current intensities to San Simón Bay and the correlation values obtained were around 0.63 for the main axis direction. The differences between observed and modelled data in Rande Strait could be owing to several causes. Thus, the HADCP was located close to the coast in a narrow strait and within a river discharge point, therefore hydrodynamic structures produced by the shoreline may not be properly represented by the model. Moreover, small bathymetric errors could also be very important in this area.

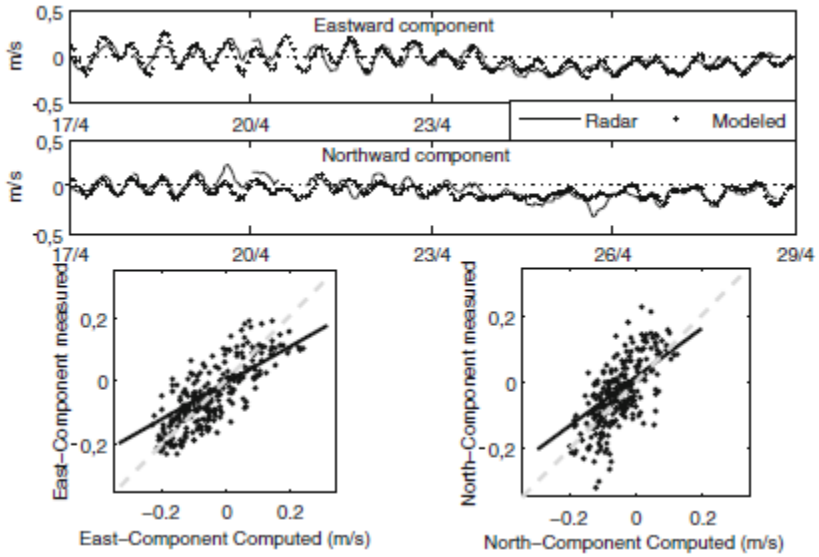

Figure 4.2: Time evolution of measured surface currents by HF-RADAR and modelled results for the same period (P3, April 2011). Source: [42]

Regarding to simulated temperature and salinity validation, modelled temperature profiles presented good agreement with measured profiles, although eventual errors were detected in salinity. The model seemed to reproduce the stratification processes

related to freshwater discharge reasonably and indicated small relative errors, as well as, situations with almost well-mixing in the entire water column. Noticeable errors were found on P1 salinity profiles, which were probably generated by an incorrect description of the continental run-off, time variability river flow, or divergences in the vertical mixing profile given by the turbulent closure scheme used within the model.

The analysis of the three validation periods (P1, P2, and P3) described above shows important temporal variability for atmospheric forcing and boundary conditions. Therefore, four periods of 3 days (prediction time designed in the operational system) representing the main ocean atmosphere patterns in the region, were selected for the sensitivity analysis. Thus, not only sensitivity to different variables was under study but also the relative importance of each one with regard to the atmospheric and boundary conditions in the area.

The sensitivity analysis took three variables into account: sea level, currents at open boundary conditions, and winds (two different configurations). The results indicated that the most important source of errors on simulated surface currents was wind. Errors on open boundary conditions seemed to be limited on the outermost part of the estuary.

Taking into account the aforementioned results, it is considered that ROMS_AGRIF hydrodynamic numerical model has been successfully calibrated for the different simulation periods abovementioned. Consequently, the numerical model is applicable for the assessment of the tidal current power capacity of the Ría de Vigo.

4.2. Energy extraction from marine currents conversion

Marine currents are a form of kinetic energy and offer an energy resource similar to wind. The considerations regarding wind turbines can be extended to marine current turbines [43]. The power output of a tidal current turbine is the kinetic energy of a fluid in a stream tube, which diameter is equal to the diameter of the turbine rotor. This power is given by:

$$P = \frac{1}{2}\rho A V^3 \tag{4.10}$$

Where P is the total power output from the turbine in Watts, ρ (kg/m^3) is the density of the fluid, A (m^2) is the cross-sectional area of the rotor blades and V (m/s) is the flow velocity averaged over the section.

The power is proportional to the cube of the velocity of the fluid; hence the energy production is highly dependent on the variability of the flow speed. Additionally, the extractable power is also proportional to the density of the fluid, which for this study was considered 1025 kg/m^3, and is thus approximately 800 times the density of the air. This means that, for an equal cross-sectional area and when considered at appropriately rated speeds, the power produced by a tidal energy converter will be significantly higher than that produced by a wind energy converter. Consequently,

smaller, and therefore more manageable, tidal converters can be deployed in comparison to enormous wind turbines; however, tidal converters can only extract a fraction of the power output due to Betz's law and the mechanical losses in the turbines.

To analyse the power output that a tidal current turbine can harness, theory from the classic analysis of wind power extraction is generally used. Betz defined the efficiency of a turbine as the ratio of the turbine power to the power of the unconstrained uniform flow through the turbine area [44]. In general, this ratio is known as the power coefficient C_p, defined by:

$$C_p = \frac{P'}{\frac{1}{2}\rho A V^3}$$

(4.11)

Where P' is the power developed by the generator. According to Betz's law, for all wind turbines currently in operation $C_p < 0.59$. Similarly, the power coefficient can also be applied for tidal current turbines, and is estimated to be in the range 0.3 – 0.5 [45][46]. Notwithstanding, some researches showed that turbines in tidal farms can produce enough power to meet a stricter definition of what it means to exceed the Betz limit [47]. The value of the power coefficient and therefore, the efficiency of the tidal current turbine, depends on several factors: type of turbine (i.e. vertical or horizontal axis turbine), pitch angle of the blades of the turbine [48], relative position of the turbine within an array farm deployment [49], variability of the incident flow speed, energy generation capacity of the tidal currents in relation with that of the turbine, and many others. Consequently, the power that a tidal current turbine can harness is modified as follows:

$$P = C_p \frac{1}{2}\rho A V^3$$

(4.12)

4.3. Methodology criteria

The methodology steps taken to generate, validate and apply the results of the numerical model, and therefore to assess the tidal current energy potential of the study area of the Ría de Vigo, are the following (*Figure 4.3*):

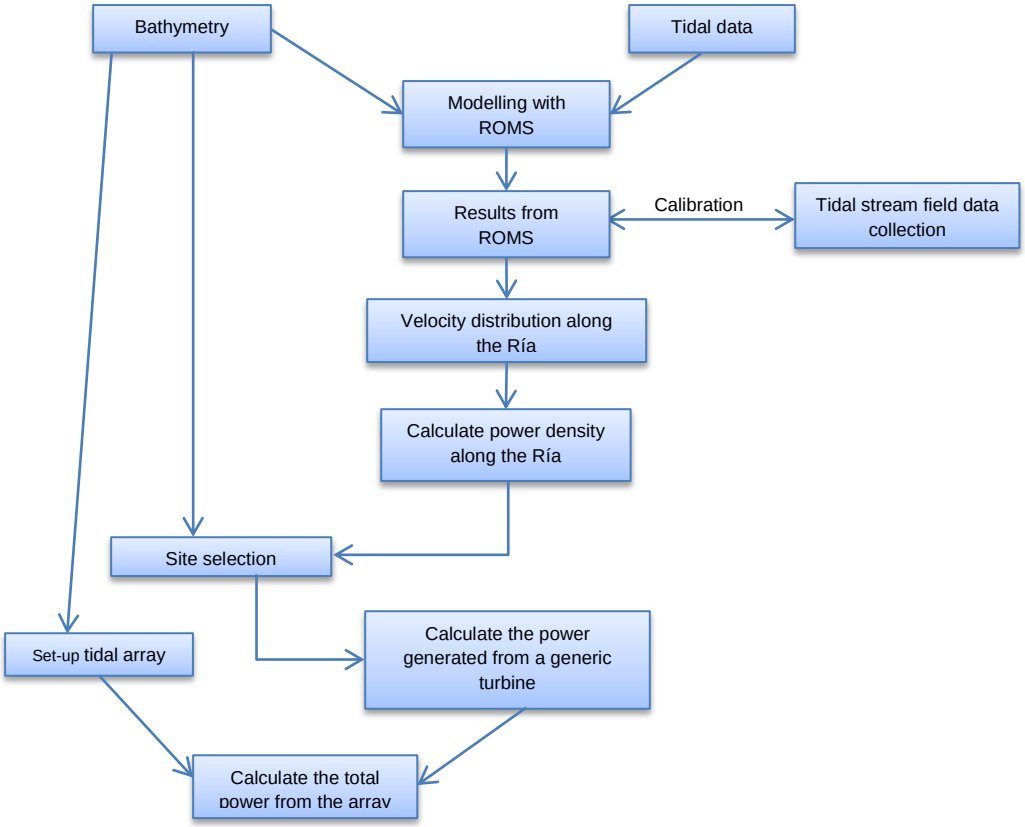

Figure 4.3: Flowchart of resource estimation methodology

Bathymetric survey: For this present research, as it can be considered as a prefeasibility assessment [50], the bathymetry data is recommended to be from a data set with spacing soundings of approximately 100 m. In this case, it has been adapted to the mesh of 150 m spacing provided by Meteogalicia. The map representing the bathymetric contours (*Figure 3.2*) gave a first idea to identify the suitable areas for the implementation of tidal energy convertors, and helped to determine any feature that could impact on the project's feasibility.

Tidal data: Reliable tidal range and tidal current data is basic to perform the hydrodynamic model adequately, as well as to calibrate and validate the model. Data were provided by Meteogalicia.

Modelling: The hydrodynamic model used in the present study is ROMS_AGRIF (afore explained) and has provided the velocity distribution along the Ría, which allowed the analysis of the tidal current potential of the area. Due to the prefeasibility approach of the research, the 3D numerical model has been used as a vertically averaged 2DH model and the distribution of the velocities has been integrated along the vertical.

Calibration: The model used was calibrated and validated against tidal current data from a field survey [42], as mentioned in the previous section.

Output data: Time, location within the grid mesh (latitude and longitude in WGS 84), velocities in the 2 horizontal directions (vertically averaged) and cell depth were recorded for each time step.

Data analysis: The distribution of the tidal current velocities in the inner Ría has been represented. Flow velocity vectors at mid-ebb and mid-flood of a mean spring tide were depicted to show where the largest currents occurred. Thereupon, power density maps were represented to reveal which areas were the most powerful over a tidal cycle.

Site selection: Some general principles for tidal current turbine site selection were noted. Generally, higher currents are found in channels or in constrictions between islands (characterized by fast and rectilinear flows). Headlands, estuaries or narrow entrances to enclosed tidal lakes, are also spots that usually present appropriate features for tidal power extraction. To reduce the risk of weather-induced delays and to maximise time available for installation and servicing, the selected site should be close to the coast, near a suitable electrical network connection on the shore and not too exposed to open sea waves and wind. Furthermore, it should also avoid sensitive environmental sites. The key criteria was to set a minimum mean spring tide velocity, 1.5 m/s, in order to achieve an economic size of rotor [51]. A depth restriction of minimum 15 m was considered to provide adequate space for a turbine rotor. The power output a tidal turbine can generate is directly related to the power density of the resource plus the size of the rotor of the turbine. Turbines with big diameters will produce more energy than those with small ones. Shallow locations (hence small rotor diameters) with greater power density (W/m^2) potentially produce less power output (W) than deeper locations (big rotor diameters) with lower power density. Therefore, the chosen location for tidal turbine technology deployment was the one that provided the highest power output for a tidal cycle, taking into account power density and installable rotor diameter (which varies with depth).

Tidal current turbine energy extraction: Given the prefeasibility character of the present work, no tidal current turbine has been designed or tested specially for the area of study. Methodology for generic tidal turbines has been used to calculate the electrical power curve of the device, the mean annual electrical power, as well as the annual energy production.

Display of a turbine farm: Two different methods were used to calculate the energy that could be generated by a tidal current turbine array: the farm method and the flux method. The performance of the turbine farm depends on the array structure and also on the device spacing. These factors were briefly analysed in the present study to provide a rough idea on how to design a commercial scale tidal turbine farm.

Chapter V

Analysis of the tidal energy resource

In the previous chapters tidal power energy has been presented and tidal power energy extraction has also been described. Data and methodology used for analysing the energy potential of a specific region (Ría de Vigo) have also been outlined and modelling data validated. The model may now be used to calculate the tidal flow velocities around the embayment. This chapter presents the assessment of the resource and criteria to perform site selection for tidal energy convertors (TEC) deployment.

5.1. Flow velocity vectors

The first step to acquire an initial perspective of the resource capacity is to represent the distribution of the tidal current velocities within the estuary. Flow velocity vectors at mid-ebb and mid-flood of a mean spring tide have been depicted to show where the largest currents occurred (*Figure 5.1* and *Figure 5.2*).

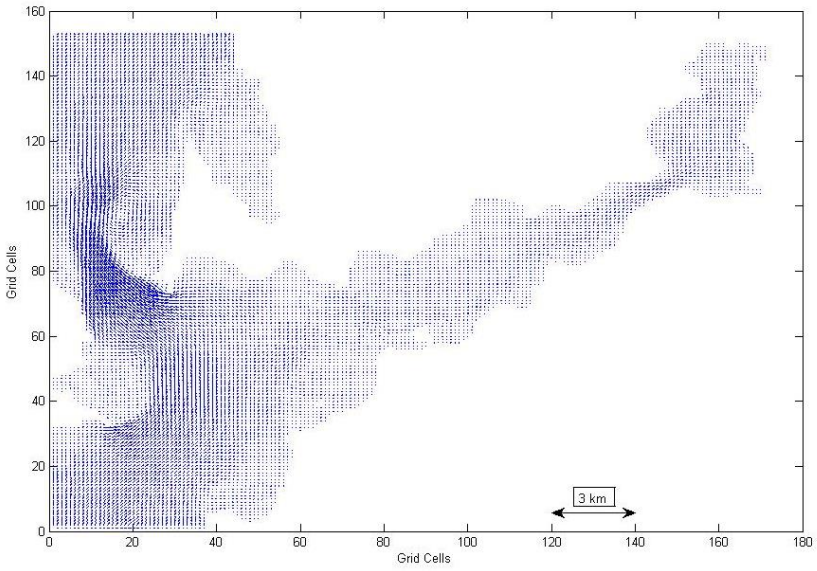

Figure 5.1: Flow velocity vectors in the Ría de Vigo at mid-flood of a mean spring tide (the coordinate axes represent the grid cells of the model for the study area)

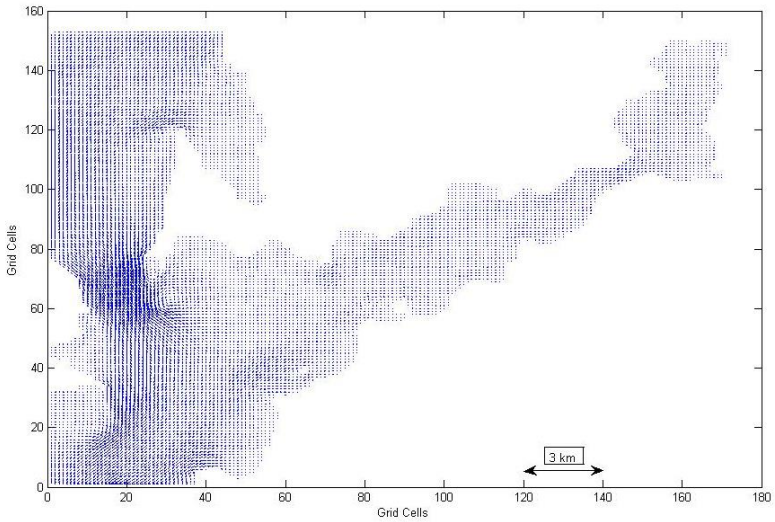

Figure 5.2: Flow velocity vectors in the Ría de Vigo at mid-ebb of a mean spring tide (the coordinate axes represent the grid cells of the model for the study area)

For both cases, the highest velocities befell in the outer part of the ría, in the strait between the Cíes Islands and the northern peninsula, in the constriction imposed on the flow by the approaching margins. In the inner ría, current velocities are lower due to friction caused by the decreasing depth.

The largest tidal currents are shown in more detail in *Figure 5.3* and *Figure 5.4*.

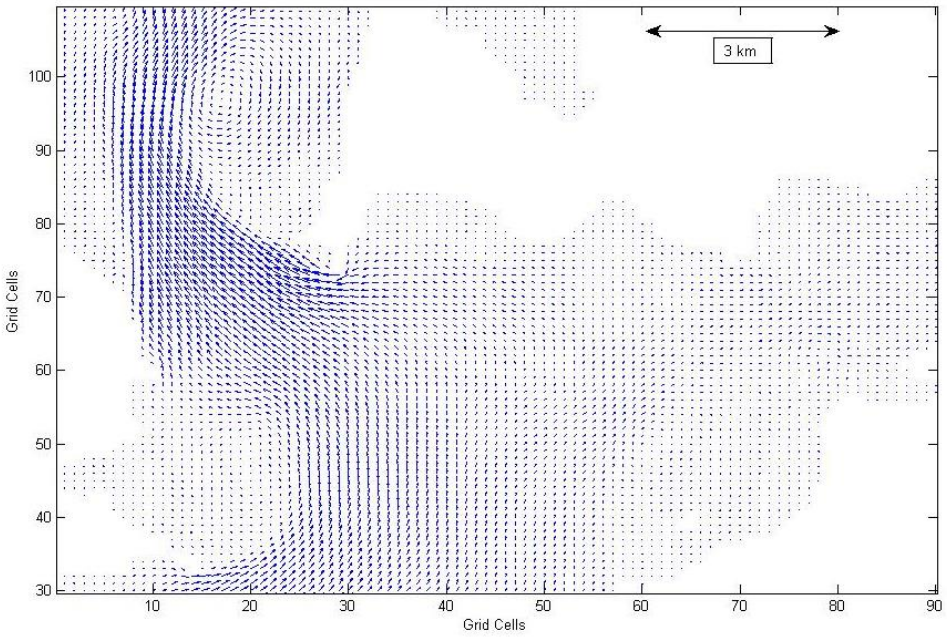

Figure 5.3: Detailed view of flow velocity vectors at mid-flood of a mean spring tide (the coordinate axes represent the grid cells of the model for the study area)

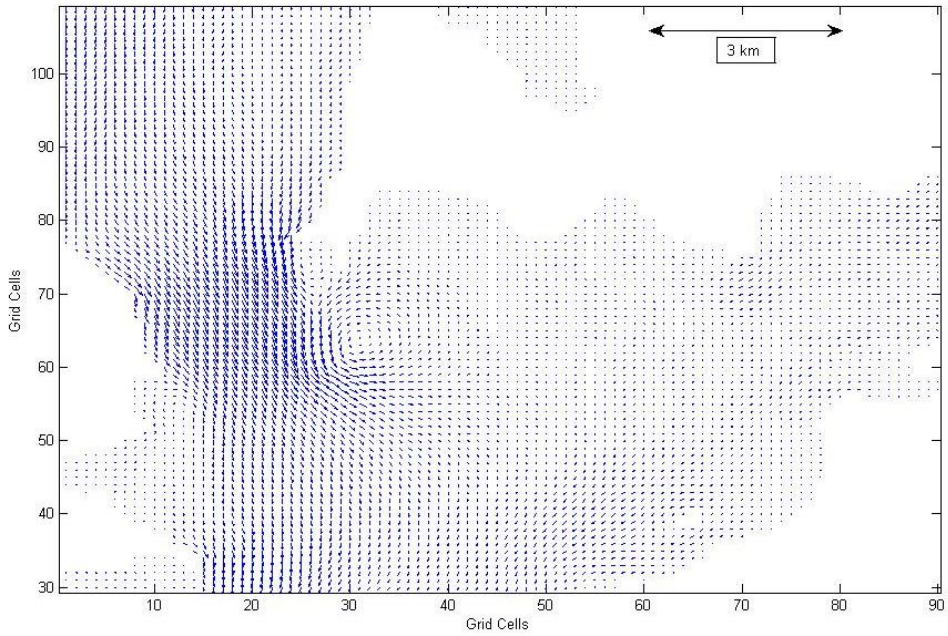

Figure 5.4: Detailed view of flow velocity vectors at mid-flood of a mean spring tide (the coordinate axes represent the grid cells of the model for the study area)

When the tide rises (*Figure 5.3*), water from the ocean enters the estuary increasing in velocity at the strait between the Cíes Islands and the peninsula. The tidal currents follow the strait towards the estuary located in the north, Ría de Pontevedra. Eddies can be observed behind the tip of the peninsula.

Moreover, when the tide falls (*Figure 5.4*), tidal currents travel inversely along the strait, from north to south, increasing their velocity as it narrows and heading towards the open sea.

To quantify the magnitude of the currents, flow velocity module maps have been represented for both cases at mid-ebb and mid-flood of a mean spring tide (*Figure 5.5* and *Figure 5.6*).

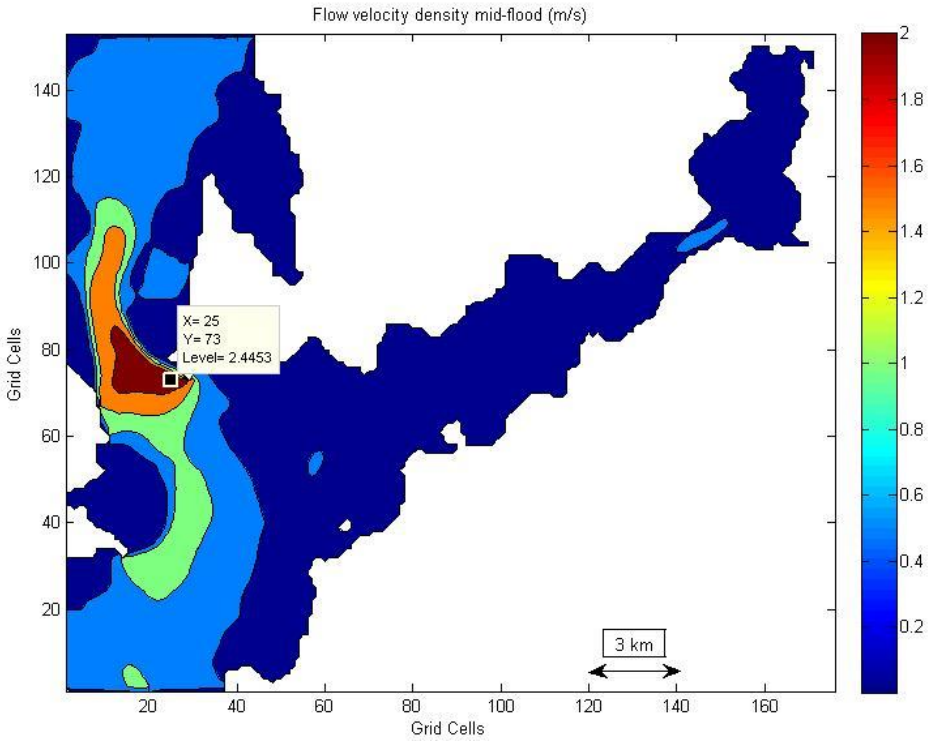

Figure 5.5: Flow velocity module (m/s) at mid-flood of a mean spring tide (the coordinate axes represent the grid cells of the model for the study area)

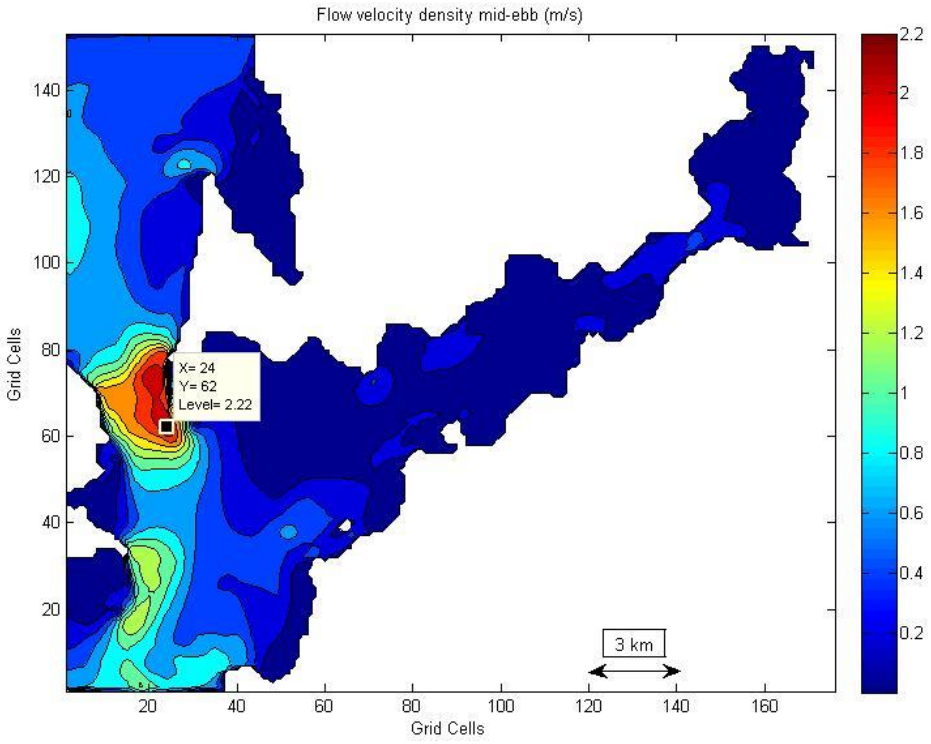

Figure 5.6: Flow velocity module (m/s) at mid-ebb of a mean spring tide (the coordinate axes represent the grid cells of the model for the study area)

The highest velocities occur in the strait between the Cíes Islands and the peninsula. The current velocities in the inner ría including San Simón Bay are lower than 1 m/s, which is the minimum value for economic operation of a tidal stream power plant according to the literature [52]. The highest velocities in the strait are around 2 m/s for both mid-flood and mid-ebb. It is generally considered that a mean spring peak tidal current of at least 1.5 or 2 m/s is required for tidal stream power to be worth exploiting [53]. The largest current magnitude within each semidiurnal cycle takes place during the flood (*Figure 5.5*), with a value of 2.5 m/s and within close proximity to the tip of the peninsula. However, at the ebb (*Figure 5.6*), the highest flow velocity is slightly lower, with a maximum value of 2.2 m/s and located approximately 1 km more south. Generally, semidiurnal tides have one semidiurnal cycle with larger currents. In this case, for all the study area, the velocity modules are lower during ebb; similar occurrence as in another assessment completed in a nearby estuary, Ría de Muros [13].

5.2. Power density

As explained in Chapter 2 and Chapter 4, the tidal power extractable is directly related to the cube of the velocity of the tidal stream. Considering the following formula:

$$Pd = \frac{1}{2}\rho V^3 \ \ (W/m^2)$$

(5.1)

Where P_d refers to the power density output per area swept by the blades of a turbine. The density of the sea water ρ is considered 1025 kg/m^3. V (m/s) is the velocity of the tidal stream.

The power density for both semidiurnal cycles (mid-flood and mid-ebb of a mean spring tide) has been represented in *Figure 5.7* and *Figure 5.8*. As expected, the highest power peaks are produced at the same locations where the higher velocities occurred, and have a maximum peak value of 7.5 kW/m^2 during the flood and 5.6 kW/m^2 during the ebb.

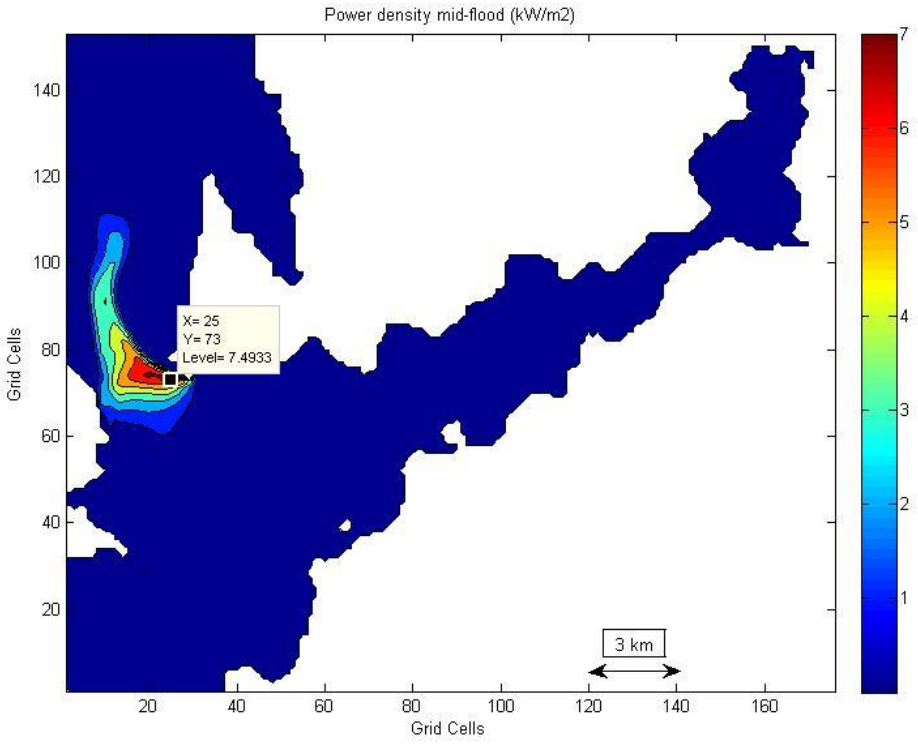

Figure 5.7: Power density (kW/m^2) at mid-flood of a mean spring tide (the coordinate axes represent the grid cells of the model for the study area)

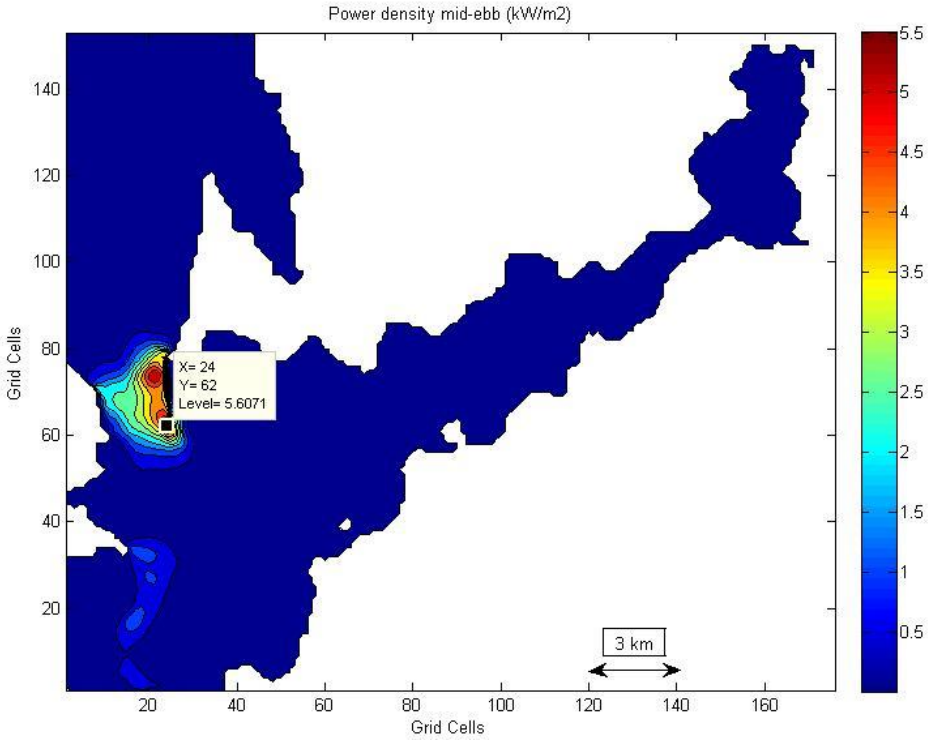

Figure 5.8: Power density (kW/m^2) at mid-ebb of a mean spring tide (the coordinate axes represent the grid cells of the model for the study area)

5.3. Site selection: Power-bathymetry-diameter matrix

The selection of the best tidal energy exploitation site should be made representing the average power density of an entire tidal cycle since a tidal stream power plant works continuously and uninterruptedly.

The average power density (APD) available across the surface area considered has been calculated directly from the time series, obtained from the model, following the equation below:

$$APD = \frac{1}{2}\frac{1}{N}\rho\sum_{i=1}^{N}\left(V_i^3\right) = \frac{1}{2}\rho V_{rmc}^3 \ (W/m^2) \quad and \quad V_{rm} = \sqrt[3]{\frac{1}{N}\sum_{i=1}^{1}(V_i^3)} \tag{5.2}$$

Where *i* is the index of the 1 hour increments (time steps considered in the model) and *N* the total time steps (673 hours of a tidal cycle); V_{rmc} is the root mean cubed velocity (m/s). The average power density distribution is represented in *Figure 5.9*.

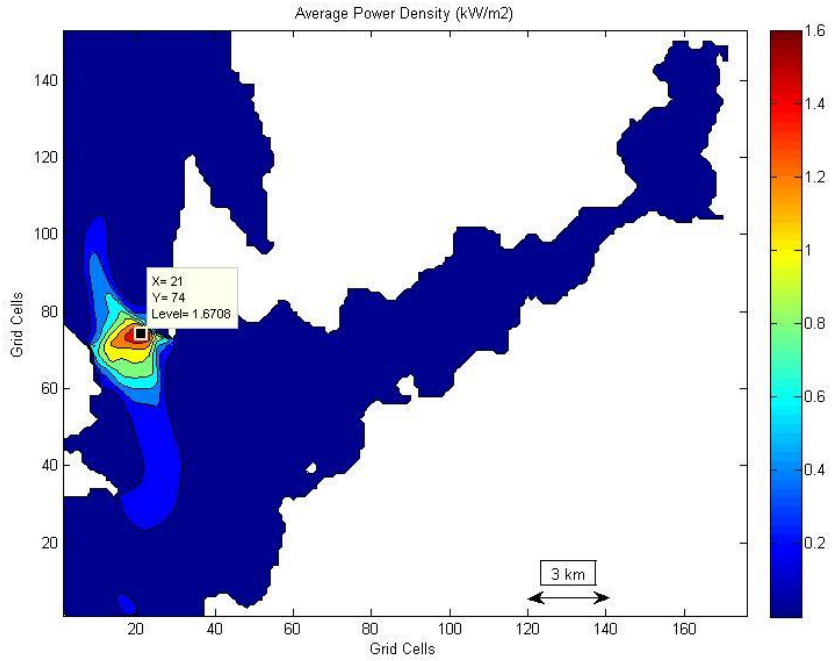

Figure 5.9: Average power density (kW/m^2) of a tidal cycle (the coordinate axes represent the grid cells of the model for the study area)

The strait between the Cíes Islands and the peninsula is the area with more potential in the existing estuary, with a maximum value of 1.7 kW/m^2, higher than in other areas where this resource was assessed [13] [53][54].

Nevertheless, the average power density represented in *Figure 5.9* does not take into account the area swept by the blades of the turbine. The extractable power directly depends on the cross section of the turbine and consequently on the dimension of its

diameter (Equation 4.10). Greater diameters will produce higher power. The size of the turbines that can be installed depends on the bathymetry of the area of study (*Figure 5.10*); hence it is necessary to know if the potential areas have enough depth to allow the implementation of turbines. Initially, a depth restriction of minimum 15 m has been considered to provide adequate space for a turbine rotor.

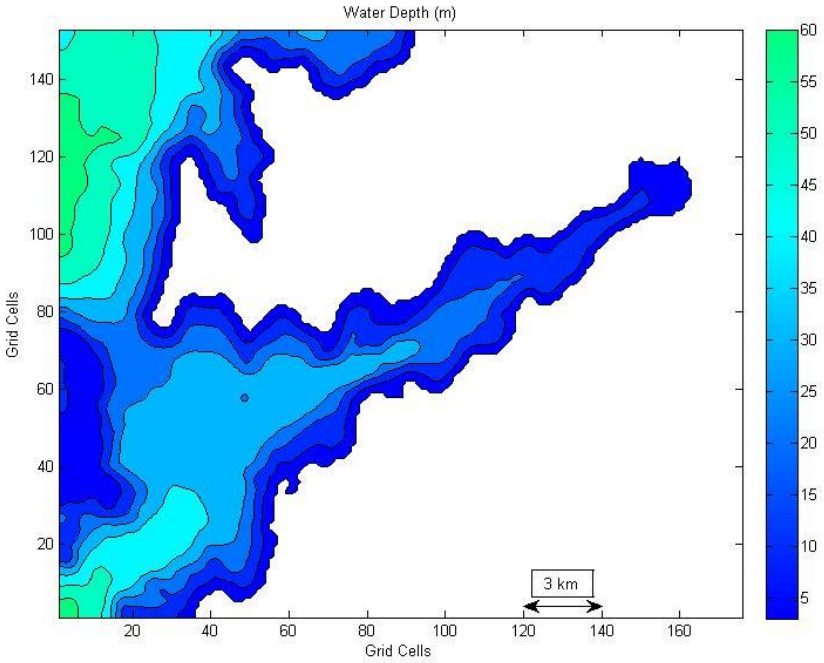

Figure 5.10: Bathymetry of the Ría de Vigo (the coordinate axes represent the grid cells of the model for the study area)

The area with the greatest potential regarding power density (depicted in *Figure 5.9*) has a water depth in a range of 25 – 50 m.

Although no single tidal stream technology is currently considered as the “standard” technology, and therefore the most appropriate for resource assessment, the most advanced tidal stream technology type in use is the horizontal axis turbine. Thus, a horizontal axis turbine should be considered in the case that no specific tidal energy converter (TEC) has been identified.

As a specific TEC has not been identified, generic characteristics can be used for the following items [50]:

Maximum rotor diameter: A reasonable diameter has to be considered depending on the state of the technology. The diameter is believed to be currently limited to 20 - 25 m for a standard horizontal axis turbine. As technology matures, larger, and thus more efficient, rotor sizes may be possible.

Top clearance: A minimum 5 m top clearance is normally recommended to allow for recreational activities (small boats, swimmers, etc.), and to minimise turbulence and wave loading effects on the TEC, as well as damage from floating materials.

Bottom clearance: A bottom clearance of 25% of the water's depth or 5 m is recommended. The greatest of both values should be considered as a minimum to prevent the impact on the rotor of potentially TEC-damaging materials that are moved along the seabed by the currents, and to minimise turbulence and shear loading from the bottom boundary layer (*Figure 5.11*).

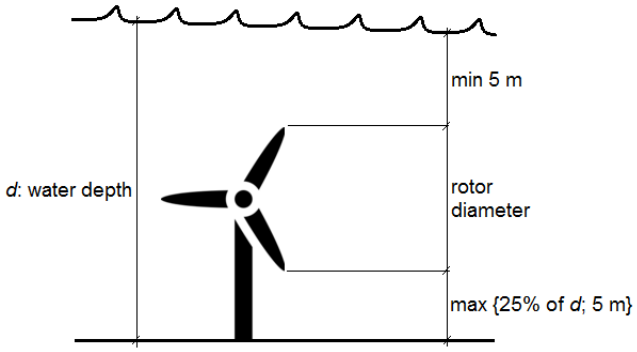

Figure 5.11: Top and bottom clearance recommendations for TEC turbine deployment

Considering the mentioned items, the available vertical space for tidal turbines (or potential diameter) has been calculated directly from the time series obtained by the model and is represented in *Figure 5.12*.

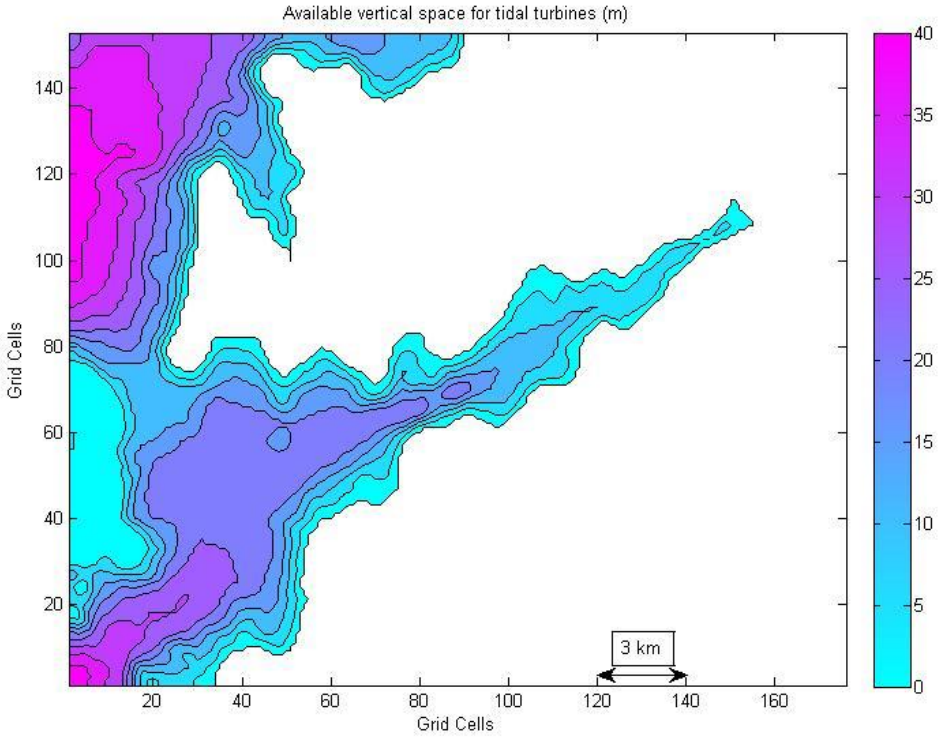

Figure 5.12: Available vertical space for TEC deployment (m) (the coordinate axes represent the grid cells of the model for the study area)

The above stated potential area (in the strait) can hold rotor diameters from 10 to 40 m, albeit a diameter limit of 21 m has been established considering the aforementioned generic specifications and also the size of the commercial TEC turbines inventoried in Chapter II. Accordingly, the available vertical space for tidal turbines with diameter limitation is shown in *Figure 5.13*

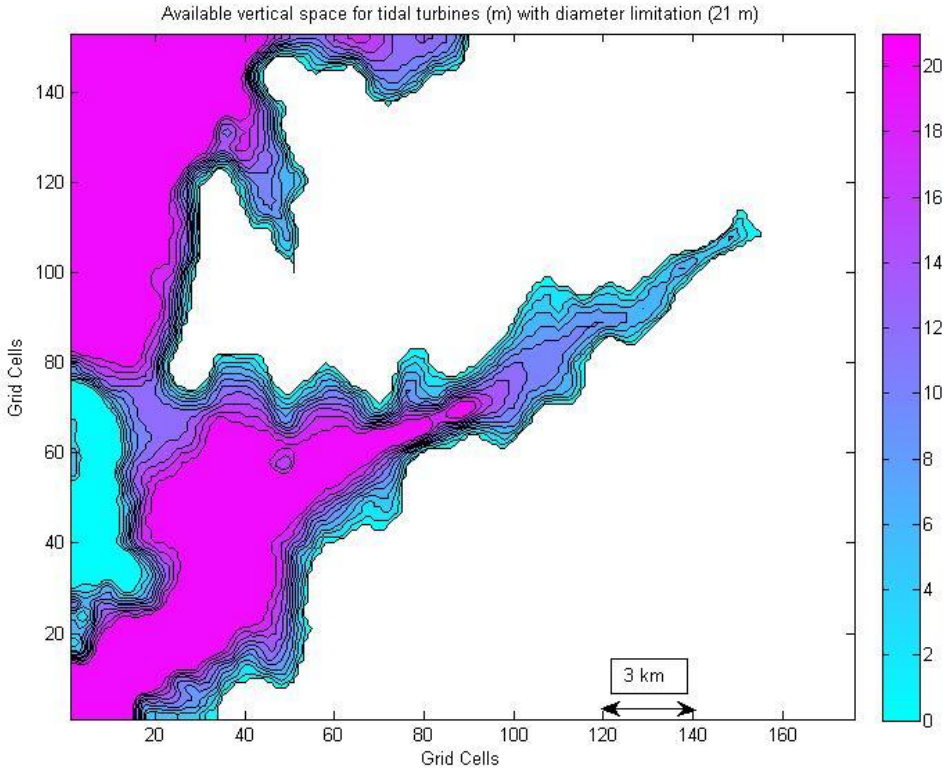

Figure 5.13: Available vertical space for TEC deployment with diameter limitation (m) (the coordinate axes represent the grid cells of the model for the study area)

The potential area in the existing estuary deemed to be suitable for installing tidal stream turbines is the site that provides the highest power output for a tidal cycle, taking into account the average power density (*Figure 5.9*) and the installable rotor diameter (*Figure 5.13*). Following the Equation 4.10 these two components have been assembled in *Figure 5.14* to represent the potential sites for TEC turbines deployment. The selected site presents a power output of 265 kW.

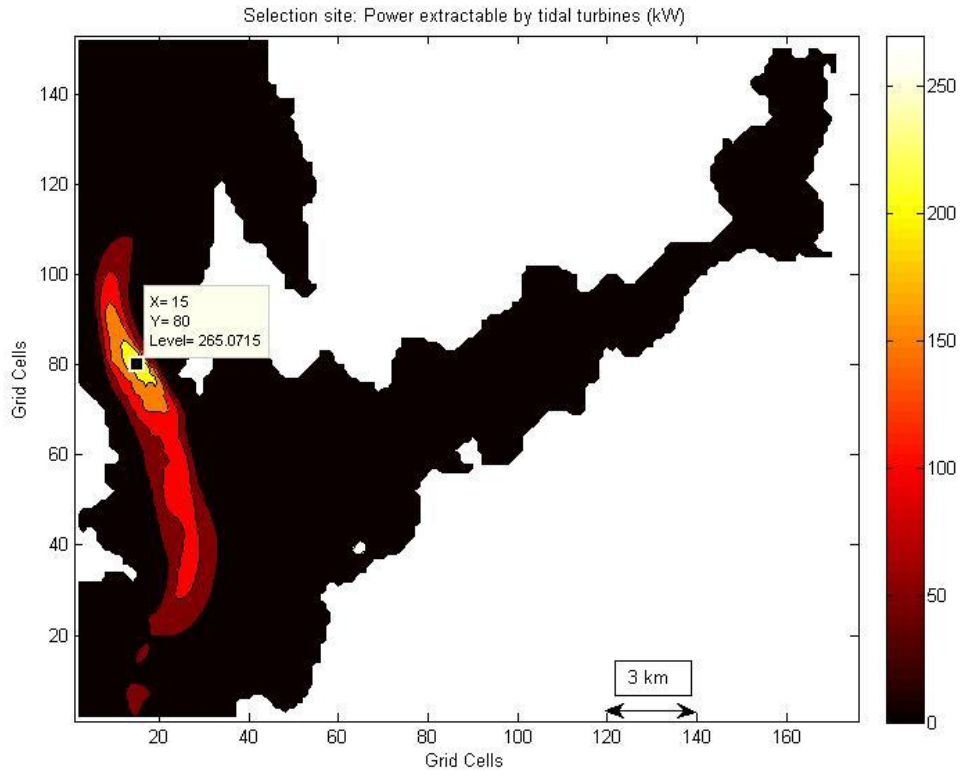

Figure 5.14: Power output extractable by TEC turbines (kW) (the coordinate axes represent the grid cells of the model for the study area)

5.4. Selected site description

The chosen site for TEC turbine deployment is located at 42°15'16.7"N 8°53'23.9"W coordinates (*Figure 5.15*), at approximately 1.2 km from the Costa da Vela (at the peninsula) and at 1.7 km from the Cíes Islands. Certainly, the site offers adequate space to allow ship navigation along the strait, as well as ensures easy transport of electricity, due to the location is considered a near-shore site (situated at less than 5 km from the coast) [43] and it is close to the energy transport grids.

Figure 5.15: Selected site location visualised through Google Earth

The selected site presents the following characteristics:

Grid Cell position		Geographic Cartesian coordinates		Water depth	Diameter installable	Mean spring tide episode	
x	y	latitude	longitude	(m)	(m)	(step)	(days)
15	80	42.254631	-8.8899698	35.24	21	182	7.54

Table 5.1: Selected site features

The next table indicates the velocity and power magnitudes at selected site during the mean spring peak (V_{msp} and P_{msp}) and during an entire tidal cycle (*AVM* and *APD*).

V_{msp}	*Average Velocity Module*	P_{msp}	*Average Power Density*
(m/s)	(m/s)	(kW/m2)	(kW/m2)
2.20	0.89	5.45	0.77

Table 5.2: Velocity and power magnitudes at selected site

The velocity magnitude and the power density at selected site are shown in *Figure 5.16* and *Figure 5.17* during a 28-day period so as to cover the spring-neap variation.

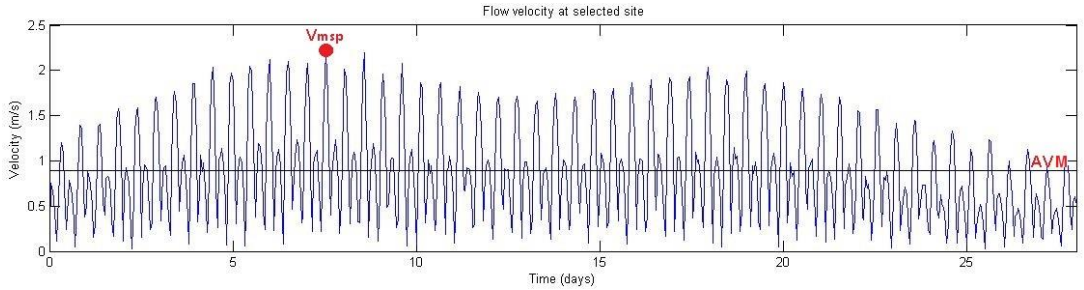

Figure 5.16: Flow velocity (m/s) at selected site throughout a 28-day tidal cycle

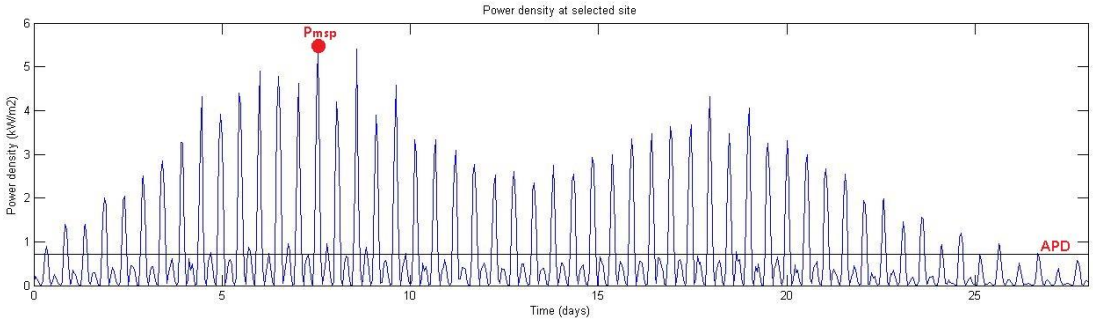

Figure 5.17: Power density (kW/m^2) at selected site throughout a 28-day tidal cycle

The power peak values during the flood are much larger than those during the ebb due to the difference in peak velocity between them is amplified by the cubic exponent. resulting in a large disparity in power density values.

For the 28-day period considered the energy per square meter of turbine aperture (the energy density) available at the selected point is the area under the curve in *Figure 5.17*. A numerical integration yields 515.02 kWh/m^2 for the 28-day period. The annual power energy available at the selected site results in 6.71 MWh/m^2.

Chapter VI

Practical application for a turbine array deployment

The essential part in designing a tidal plant is the device choice. Owing to the fact that the technology for harnessing energy from tidal currents is at its early stage, the device selection faces a number of main difficulties; the unfamiliarity of methods involved in installing and operating TEC turbines on an industrial scale, the absence of references and the small number of experienced construction contractors in similar technology, without disregarding the financial and technical uncertainty linked to developing a tidal device adapted to a specific site as Ría de Vigo.

At this stage there is no knowledge about which TEC turbine generally performs the best, as each device will perform differently at each particular site. Therefore, it has been decided to consider a generic TEC turbine and not to select any specific device for the practical application to a turbine array deployment in the Ría de Vigo. As no single tidal stream technology is currently considered the generic or standard, the horizontal axis tidal current turbine (HATCT) has been assumed for all the calculations within the farm design process. The HATCT is the most developed tidal current energy extraction device [51]. Many developments on the field have taken place during the recent years, moving from model testing to prototype development and installation.

Two HATCT developers have been consulted; Lunar Energy [55] and Marine Current Turbines (MCT) [56]. There is no intent to compare them, as each developer proposes a HATCT device design quite different from the other. They have been chosen since their principal characteristics make them suitable to be deployed in the study embayment, though this is not the aim of this study. The purpose is to explain the different components of each device, as both are solid developed designs, to increase the confidence level of the present assessment and to understand the installation, operation and maintenance activities distinctive of a TEC turbine farm.

With the aim of giving an economical approach to the study here-in, data provided by MCT have been used to calculate the approximate capital cost breakdown of a tidal plant deployed in the selected site.

Furthermore, the impacts on the marine environment caused by the operation of a tidal stream farm are an important issue that must be addressed in terms of tidal farm designing.

6.1. Tidal energy harnessed by tidal turbines

The total power in the flow at the selected site cannot be extracted for energy production due to Betz limit and many other potential losses in the power extraction such hydrodynamic losses, transmission losses and generator losses [57]. These limitations, regarding turbine efficiency, are accounted for via an overall power coefficient C_p (described in Chapter IV).

The main goals of this section are:

- To measure and describe the resource by deriving a velocity distribution for the selected site.
- To understand the potential for the power extraction of an array of TEC turbines by combining the velocity distribution with the power curve of the TEC turbine.
- To ensure that the tidal resource available is not over extracted.
- To estimate the annual energy output, once the velocity distribution has been calculated and after applying it to the TEC turbine's power curve.

6.1.1. Velocity distribution

Tidal currents vary with time. Currents at the selected site are characterised by a distribution of velocities, as shown in *Figure 6.1*, which is used to calculate the annual performance of the device at the site. Since power density varies with the cube of velocity, the mean electrical power cannot be obtained directly by substituting the mean current speed (or *AVM*) into the power density equation (4.10). Once the distribution of velocities is known for the selected site, the distribution of power densities can be readily calculated and averaged to find the average power density for that site (explained in section 6.1.3).

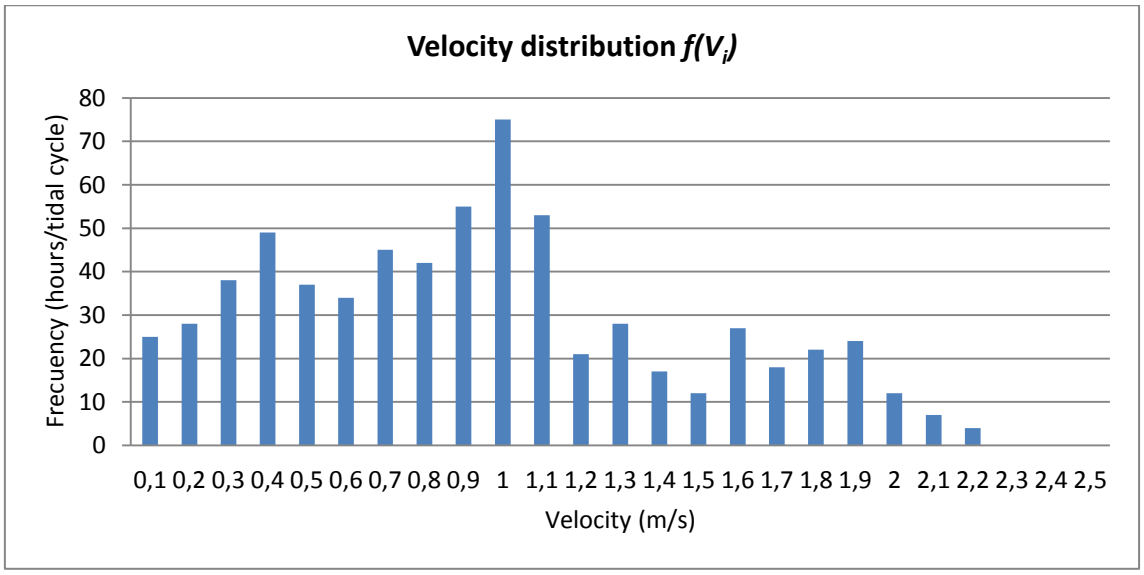

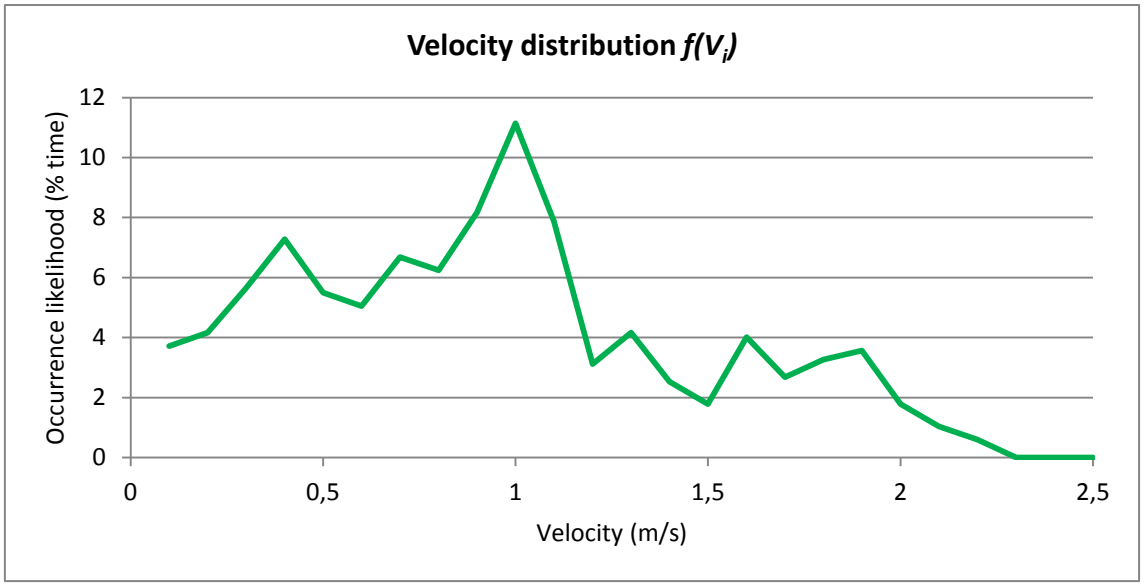

Figure 6.1: Velocity distribution histogram and chart at the selected site, for an entire 28-day tidal cycle

6.1.2. Power curve

The power recovery efficiency and turbine performance can be estimated using the simplified model of a generic tidal current device described below. The calculation addresses the power conversion efficiency of each step in the process, beginning with the power of the flowing water stream and proceeding through the turbine, drivetrain, generator and power conditioning steps [58].

Turbine efficiency varies with the velocity of water flow. As a specific TEC turbine has not been identified, draft methodology from the literature [50] has been used to obtain the power curve for a generic device (a horizontal axis turbine with a 21m diameter has been considered for the calculations). The power curve calculated here is not regarded as accurate, but is sufficient to determine whether the energy that is planned to be extracted by a tidal farm does not exceed the available resource. Further studies should include power curves provided by tidal developers to better qualify and quantify the resource. The specifications considered are the following:

The cut-in speed ($V_{cut\text{-}in}$): the minimum velocity required for device operation, which is assumed constant at 0.5 m/s. This assumption greatly simplifies the analysis and does not impose significant limitations on accuracy.

The rated velocity (V_{rated}): the velocity for which the turbine has been optimized. The value of C_p varies with the current velocity for a given type of turbine, having a maximum at a particular velocity that is regarded as the rated velocity [53]. The rated velocity can be taken as 71 % of the V_{msp}.

The rotor efficiency or turbine efficiency (η_{ROTOR}): the efficiency with which the turbine extracts kinetic energy from the incoming flow. It rises from 38% at cut-in speed up to 45% at the rated velocity.

The power take-off efficiency: the sum of the efficiency of the drivetrain ($\eta_{GEARBOX}$), the generator efficiency ($\eta_{GENERATOR}$) and the power conditioning efficiency ($\eta_{POWERCONDIT}$). Multiplying the incident flow power by the rotor efficiency and the power take-off efficiency determines the electric power delivered to the grid, according to the following equation:

$$P_{electric} = P'_{av}\ A\ \eta_{ROTOR}\ \eta_{POWER\ TAKE-OFF}\quad (kW) \tag{6.1}$$

Where $\eta_{POWERTAKE-OFF} = \eta_{GEARBOX}\ \eta_{GENERATOR}\ \eta_{POWERCONDIT}$ (%) and P_{av}' (kW/m^2) is the available power density of the water passing through the area swept by the turbine blades A (m^2).

The typical values considered for the component efficiencies are:

$\eta_{GEARBOX}$ = 96%: the efficiency with which the energy extracted from the flow is delivered to the generator. Losses at this stage include friction within the gearboxes commonly used to step up the rotational speed of the turbine rotor (slow) to the rotational speed of the generator (fast).

$\eta_{GENERATOR}$ = 95%: the efficiency with which the mechanical energy input to the generator is converted to electricity. Losses are primarily due to friction.

$\eta_{POWERCONDIT}$ = 98%: the efficiency with which the electricity produced by the generator is conditioned to meet phase and voltage requirements of the local grid interconnection point. Losses are primarily electrical energy dissipated as heat.

The baseline values to calculate the power curve, taking into account the results obtained in Chapter V for the selected site, are the following:

ρ (kg/m^3)	1025	A (m^2)	346.36
V_{msp} (m/s)	2.20	$V_{cut\text{-}in}$ (m/s)	0.5
Rotor diameter (m)	21	$V_{rated} = V_{msp}\cdot 0.71$ (m/s)	1.56

Then, *Table 6.1* shows the calculation of the electrical power output as a function of flow speed for the selected site and also the obtainment of the rated power of the turbine.

Average bin velocity	**Available power** $P_{av(i)}=0.5\cdot\rho\cdot A\cdot V_i^3$		**Efficiencies**				**Electrical power per bin**
V_i (m/s)	$P_{av(i)'}$ (kW/m^2)	$P_{av(i)}$ (kW)	$\eta ROTOR$ (%)	$\eta GEARBOX$ (%)	$\eta GENERATOR$ (%)	$\eta POWERCONDIT$ (%)	$P(V_i)=P_{av(i)}\cdot\eta$ (kW)
0.1	0.001	0	0	96	95	98	0
0.2	0.004	1	0	96	95	98	0
0.3	0.014	5	0	96	95	98	0
0.4	0.033	11	0	96	95	98	0
0.5	0.064	22	38	96	95	98	8
0.6	0.111	38	39	96	95	98	13
0.7	0.176	61	40	96	95	98	22
0.8	0.262	91	41	96	95	98	33
0.9	0.374	129	42	96	95	98	49
1	0.513	178	43	96	95	98	68
1.1	0.682	236	44	96	95	98	93
1.2	0.886	307	45	96	95	98	123
1.3	1.126	390	45	96	95	98	157
1.4	1.406	487	45	96	95	98	196
1.5	1.730	599	45	96	95	98	241
1.6	2.099	727	x	96	95	98	241
1.7	2.518	872	x	96	95	98	241
1.8	2.989	1035	x	96	95	98	241
1.9	3.515	1218	x	96	95	98	241
2	4.100	1420	x	96	95	98	241
2.1	4.746	1644	x	96	95	98	241
2.2	5.457	1890	x	96	95	98	241
2.3	6.236	2160	x	96	95	98	241
2.4	7.085	2454	x	96	95	98	241
2.5	8.008	2774	x	96	95	98	241
						Turbine rated power	**241 kW**

Table 6.1: Electrical power per bin as a function of flow speed, taking into account the different efficiencies referring to electrical power production

A plot of a turbine power output (electrical power per bin) as a function of flow speed typically consists of three regions that can be appreciated in *Figure 6.2*.

I. Zero to cut-in speed
II. Cut-in speed to rated speed
III. Greater than rated speed

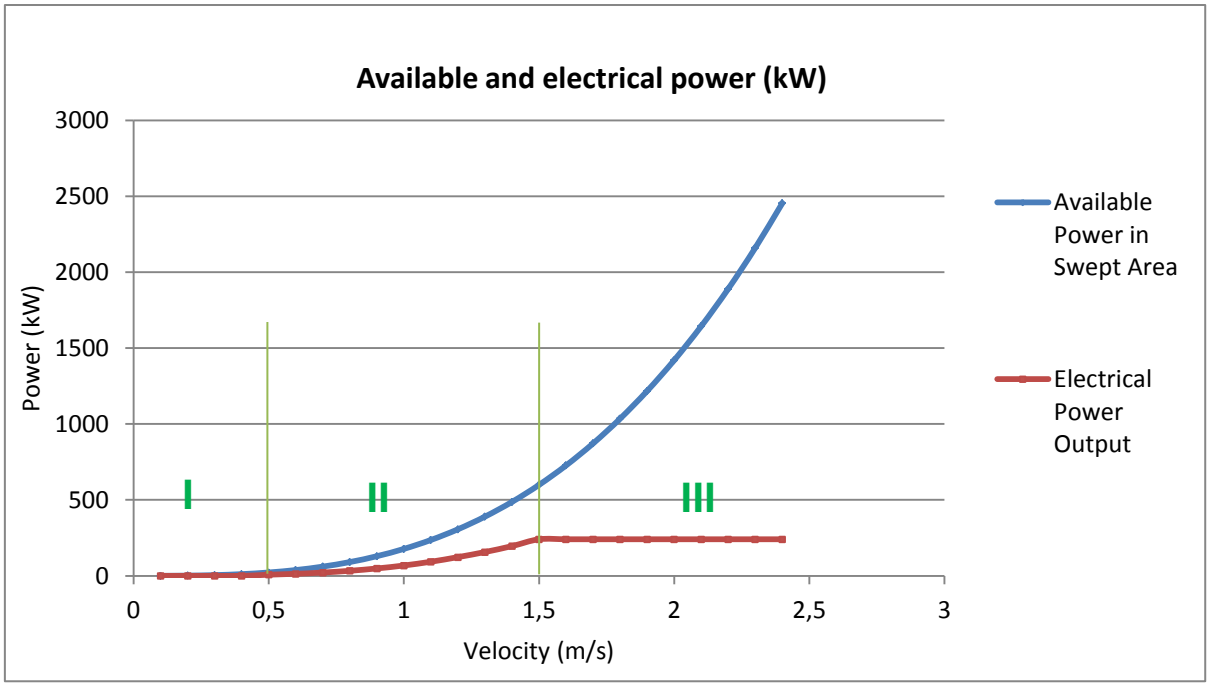

Figure 6.2: Electrical power curve

In Region I, at velocities below the cut-in speed, the turbine does not generate sufficient lift to rotate the drivetrain and thus generates no power.

In Region III, when current velocity exceeds the rated speed of the turbine, power output will be constant, typically at the rated power of the turbine, regardless of velocity.

Between the cut-in speed and rated speed, in Region II, the output of the turbine depends on conversion efficiencies, as discussed in Equation 6.1.

6.1.3 Annual energy production

For each TEC turbine, the annual energy production (*AEP*) has been calculated by combining the mean electrical power (P_{mean}) with the available hours per year:

$$AEP = 8760 \; P_{mean} \quad (kWh) \tag{6.2}$$

The mean electrical power (P_{mean}) has been obtained, as shown in *Table 6.2*, by combining the velocity distribution $f(V_i)$ (*Figure 6.1*) with the absorbed power for each velocity bin $P(V_i)$ (*Table 6.1*) calculated using the following equation:

$$P_{mean} = \sum_{i=1}^{N} P(V_i)\, f(V_i) \tag{6.3}$$

Average bin velocity V_i	**Velocity occurrence likelihood $f(V_i)$**		**Electrical power per bin $P(V_i)$**	**Mean electrical power per bin $P(V_i)x\ f(V_i)$**
(m/s)	(-)	(%)	(kW)	(kW)
0.1	25	3.71	0	0.00
0.2	28	4.16	0	0.00
0.3	38	5.65	0	0.00
0.4	49	7.28	0	0.00
0.5	37	5.50	8	0.41
0.6	34	5.05	13	0.68
0.7	45	6.69	22	1.46
0.8	42	6.24	33	2.08
0.9	55	8.17	49	3.97
1	75	11.14	68	7.60
1.1	53	7.88	93	7.32
1.2	21	3.12	123	3.85
1.3	28	4.16	157	6.53
1.4	17	2.53	196	4.95
1.5	12	1.78	241	4.30
1.6	27	4.01	241	9.67
1.7	18	2.67	241	6.44
1.8	22	3.27	241	7.88
1.9	24	3.57	241	8.59
2	12	1.78	241	4.30
2.1	7	1.04	241	2.51
2.2	4	0.59	241	1.43
2.3	0	0.00	241	0.00
2.4	0	0.00	241	0.00
2.5	0	0.00	241	0.00
N intervals	**673**		***Pmean (kW)***	**83.95**

Table 6.2: Mean electrical power

Therefore the annual energy production for a TEC turbine at the selected site is:

$$AEP = 8760h \cdot 84kW = \ 735MWh$$

To recap, *Table 6.3* summarises the characteristics of the flow power and the turbine power assessed in the present Chapter.

TEC turbine characteristics		Flow characteristics	
$V_{cut\text{-}in}$ (m/s)	0.5	V_{msp} (m/s)	2.20
V_{rated} (m/s)	1.56	AVM (m/s)	0.89
P_{rated} (kW)	241	P_{msp} (kW/m^2)	5.45
		APD (kW/m^2)	0.77
P_{mean} (kW)	84	$P_{mean\ available}$ = $APD \cdot A_{turbine}$ (kW)	265
		$AEP_{available}$' (MWh/m^2)	6.71
AEP (MWh)	735	$AEP_{available}$ (MWh)	2325

Table 6.3: Turbine and flow characteristics

The overall turbine efficiency is accounted via the power coefficient C_p (defined in Equation 4.11) as the power harnessed by the TEC turbine divided by the power available in the resource. Consequently and considering the calculations and the results above exposed the power coefficient C_p can be expressed as:

$$C_p = \frac{P_{mean}}{P_{mean\ available}} = \frac{84}{265} = 0.32 \quad or \quad \frac{AEP}{AEP_{available}} = \frac{735}{2325} = 0.32 \tag{6.4}$$

C_p = 0.32 is an acceptable value within the range mentioned in Chapter IV. The power produced by a single TEC turbine compared with the power available at the selected site during a tidal cycle is shown in *Figure 6.3* and follows Equation 6.5.

$$P_{producted} \begin{cases} 0 & if\ V_i < v_{cut-in} \\ \frac{1}{2}\rho A V_i^3 C_p & if\ v_{cut-in} \le V_i \le v_{rated} \\ P_{rated} & if\ V_i > v_{rated} \end{cases} \tag{6.5}$$

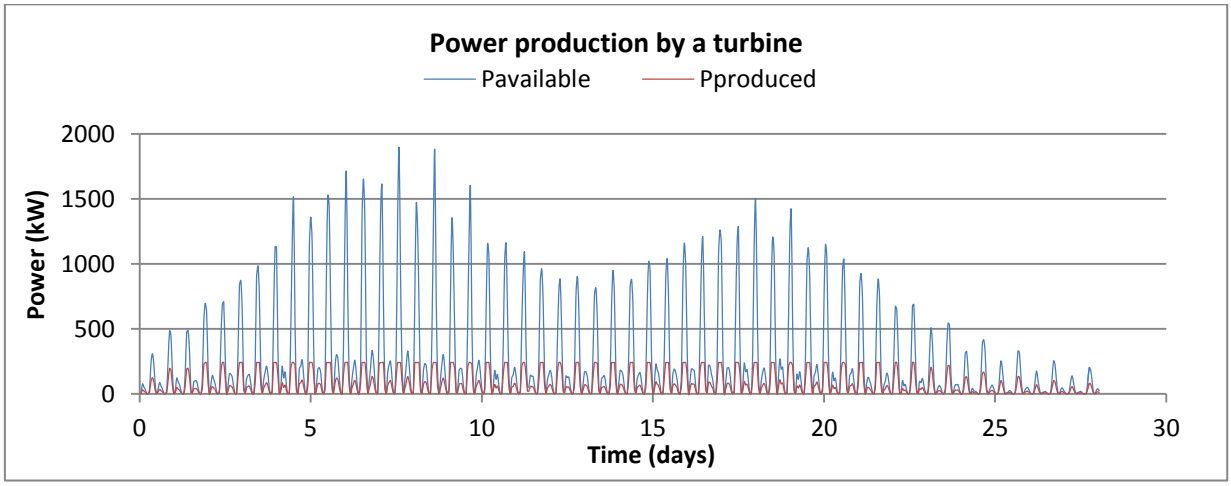

Figure 6.3: Power available and power harnessed over 28-days tidal cycle

6.2. Display of the turbine farm

This section proposes a practical application for a turbine array deployment at the selected location.

The exploitation of a tidal energy resource that implements just one single turbine can be considered illogical, since the costs of installation, onshore grid interconnection, transport, operation and maintenance, etc., are reasonably high. The cost of a single unit TEC turbine will be significantly greater than the subsequent units installed at the site. Therefore, the extraction of tidal power must be done implementing a commercial tidal plant, whose purpose is to generate cost competitive electricity for the grid without causing unacceptable environmental impacts.

Although tidal stream turbine technology is in its infancy, the technology is quickly developing industrially and academically-wise. At present, worldwide, there is no commercial stream turbine farm in operation yet, albeit many developers are on their way to deploy commercial scale tidal energy farms. Marine Current Turbines, a pioneering renewable energy developer, has successfully completed the first installation phase of the 1.2 MW SeaGen Tidal System into the fast-flowing waters of Strangford Narrow, seeking to be the world's first commercial scale tidal energy turbine deployed in Northern Ireland [56]. The Australian company Atlantis Resources has already started the construction of the largest tidal power plant in the world, the Meygen project. This project will comprise 269 tidal turbines installed on the seabed in northeast Scotland. It will have the capacity to supply nearly 175,000 households with a total potential of nearly 400 MW when completed [59].

In the study here-in, the selected site has been evaluated to design a TEC turbine array. As the construction of a tidal stream farm is expected to require an important investment it is necessary to evaluate the power output of the farm and its efficiency. Up to now, there has been no universally accepted method to quantify the tidal stream farm’s efficiency. Nevertheless there are some items that farm designers should contemplate, which are described in the following sections.

6.2.1. Extractable resource

The available energy resource is not fully extractable due to environmental concerns. The operation of a tidal farm may produce alterations of flow speed which have an important effect on the economics of energy generation in addition to possible environmental impacts. Previous work by Black & Veatch Consulting, Ltd. in conjunction with Robert Gordon University [60] suggested considering a significant impact factor (*SIF*) that represents the percentage of the total resource at a site that can be extracted without significant economic or environmental effects. *SIF* is dependent on the type of site and ranges from 10% to 50%. Despite that this document cannot give a methodology to calculate the *SIF* for a site, for the present study environmental concerns have been assumed to limit the mean extractable power to 10% of the mean kinetic power.

6.2.2. Lateral spacing

When the turbines within a tidal farm are close to each other hydrodynamic interactions will affect the performance of each turbine. Very narrow spacing may lead to negative interaction effects such as reduced power capture or increased thrust forces [61]. Despite the present lack of experience at full-scale at sea, it is possible to infer qualitative guidance for lateral inter-device spacing within arrays. Large lateral spacing within a single row array should be avoided as it will not be an efficient use of space since most tidal energy sites are generally narrow. Wider arrays will also cause a larger obstruction to maritime traffic. Therefore, there must be an optimal value regarding to lateral spacing for any situation. Some experimental studies state that an optimal lateral spacing between devices can even accelerate the flow between them [62]. This enhanced flow speed gives rise to the counterintuitive notion of a downstream row of devices producing more power than the upstream row (*Figure 6.4*). This leads to a synergistic effect, whereby an array of devices can generate more power than an equivalent number of isolated machines.

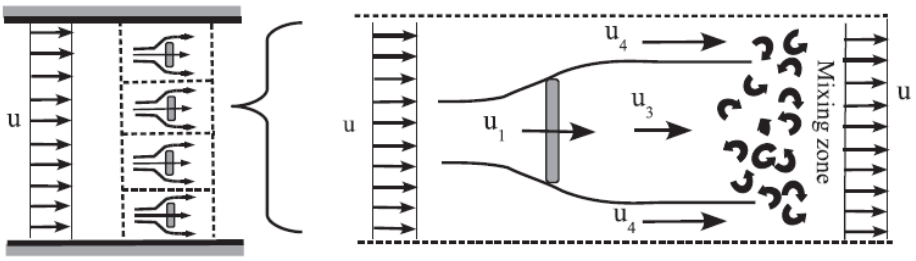

Figure 6.4: Schematic diagram of a row of turbines within a tidal farm and the flows around a turbine within the row. The ducted effect created between the turbines enhance the velocities bypassing the turbines, so that u4 ≥ u ≥ u1 ≥ u3. Source [63]

For the present study, following the draft methodology provided by [50] and considering an array of horizontal axis TEC turbines, the lateral spacing between devices (distance between axes) has been considered two and a half times the rotor diameter (2.5 d).

6.2.3. Downstream spacing

Fluid passing through a horizontal axis TEC turbine will experience a reduction in velocity across the rotor plane. Downstream of the rotor this region of fluid moves at a lower velocity than the free stream fluid and hence must expand in order to conserve momentum. This takes the form of a gradually expanding cone-shaped region downstream of the rotor that is more commonly known as the wake (*Figure 6.5*). Turbulent mixing in the boundary region between the wake and the faster moving free stream fluid serves to re-energise the wake, breaking it up and increasing the velocity. At a distance far downstream the wake will be almost completely dissipated and the flow field will closely resemble that to which existed upstream of the rotor disk. There have been previous studies investigating the wake effects and energy losses within arrays of tidal turbines. The reduced velocity deficits were measured extending beyond

the near wake region up to ten diameters downstream [62], which coincides with the recommendations provided by [50].

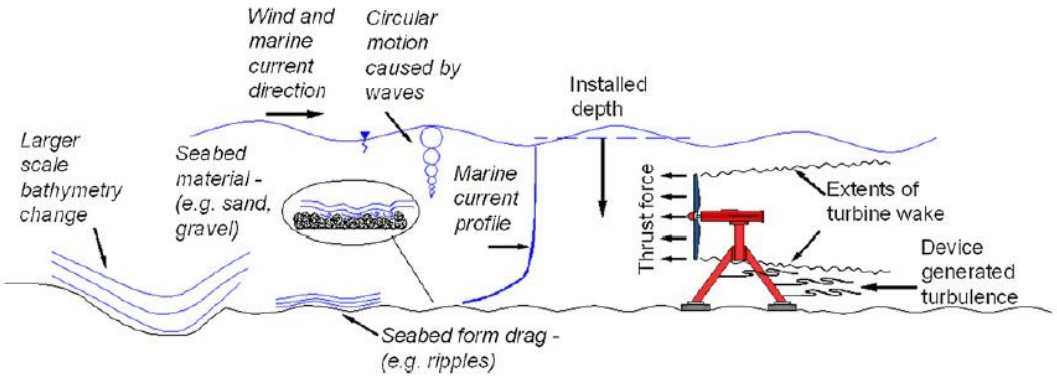

Figure 6.5: Variables that may influence the wake structure for a single TEC turbine. Source:[62]

For the present study, the downstream spacing between devices has been considered ten times the rotor diameter (10 d).

6.2.4. Others

There are many other factors concerning tidal farm design, such as the array shape, the device direction and the device tuning.

Regarding the array shape, in the proposed design, the devices have been positioned in an alternating downstream arrangement to harness the ducted effect created between the turbines shown in *Figure 6.4*. The devices within an array should be deployed facing the main tidal stream direction [64]. Furthermore, as water flow direction reverses, generally twice a day, the adjustment of the pitch of the turbine blades (tuning) becomes an essential mechanism to maximise the output of the turbines. A study of an innovative turbine with rotors rotating in opposite directions goes more in-depth into the subject [6], although it is not the scope of the present study.

6.2.5. TEC turbine array in Ría de Vigo: flux method and farm method

In general, there is no standard methodology to design a turbine farm. Considering the prefeasibility character of the study here-in, an array configuration has been proposed to describe the resource and to give a conceptual idea on farm design methodology. The configuration proposal for the existent embayment takes into account the recommendations exposed in the previous sections, which for a generic site are believed to be close to optimal, although, when modelling of wake effects is undertaken, these recommendations might be on the conservative side.

According to [50] two methods are commonly used to calculate the energy that a TEC turbine array could potentially generate; the flux method and the farm method.

The first method is based on the calculation of the incoming kinetic energy flux through the frontal cross-sectional area of a flow channel within the selected site. The resulting available resource estimate is independent of the device type, efficiency, and packing density, taking only the energy flowing in the site into account. The extractable portion of the resource is then estimated using a *SIF* (10%).

The second method calculates the energy generated by an array, obtaining the electrical energy output of each TEC turbine and adding the results.

Flux method

P_{flux} is the total power available in the cross-sectional area of the selected site considered for TEC turbine installation. It is calculated by multiplying the average power density (*APD*, calculated in 5.3) by the cross-sectional area of the selected site. If a different velocity distribution is available in several grid cells for the cross-sectional area considered, then the *APD* should be calculated for each cell.

$$P_{flux} = \sum_{i=1}^{Nc} APD_{(i)}\, d_{cell\,(i)} w_{cell\,(i)} \quad (kW) \tag{6.6}$$

Where $APD_{(i)}$ is the average power density (kW/m^2) at each grid cell, $d_{cell(i)}$ is the depth of the cell (m), $w_{cell(i)}$ is the width of the cell (m) and *Nc* is the number of cells.

Site selection made in Chapter V resulted in the location depicted in *Figure 6.6*. The selected area for TEC turbine farm deployment is also highlighted and is composed by the regions with more power potential, which are aligned perpendicularly to the main flow direction. P_{flux} has been calculated for the tidal farm, which occupies four different grid cells and has the characteristics described in *Table 6.4*.

	Power output extractable by TEC turbines (kW)										
85	172,08	192,44	206,44	198,54	156,54	99,10	61,34	49,86	41,22	33,67	24,70
84	170,48	190,73	210,50	219,64	195,77	139,42	83,07	58,47	42,19	34,44	28,02
83	170,38	189,57	209,05	228,20	226,76	189,11	124,15	75,87	49,64	36,34	30,04
82	169,85	188,45	204,78	226,03	240,67	232,24	183,32	104,78	56,44	44,50	33,49
81	167,66	186,66	199,66	219,36	240,94	256,26	241,10	165,82	85,37	50,34	37,78
80	148,78	167,79	195,97	214,40	238,09	**265,07**	254,42	211,34	141,83	75,20	42,64
79	131,16	151,64	161,14	196,20	219,05	245,64	246,38	231,76	188,43	127,54	62,84
78	103,04	138,55	149,97	166,63	187,06	208,25	231,84	227,89	209,30	169,21	103,12
77	90,13	112,97	142,24	160,04	180,91	201,12	221,95	216,39	233,94	211,99	150,45
76	79,20	103,50	119,53	136,31	155,30	173,40	190,59	207,54	195,02	208,10	185,51
75	71,26	95,74	114,29	131,78	150,38	167,76	183,57	198,87	184,26	196,95	177,07
Grid Cells	10	11	12	13	14	15	16	17	18	19	20

Figure 6.6: Power extractable at selected site (x: 15, y: 80) and surroundings. Framed grid cells represent the area considered for TEC turbine array deployment

	x	y	APD (kW/m²)	d_{cell} (m)	w_{cell} (m)	$P_{fluxcell}$ (kW)
Zone 1	14	81	0.70	37.00	150	3860.99
Zone 2	15	82	0.67	37.37	150	3758.38
Zone 3	**15**	**80**	0.77	35.24	150	4044.99
Zone 4	16	81	0.70	35.14	150	3669.23
					P_{flux}	**15333.58 kW**

Table 6.4: P_{flux} calculation of the site selected for TEC turbine array deployment

The average available power ($P_{available}$) is the product of the power flux passing through the site and the significant impact factor (*SIF*):

$$P_{available} = P_{flux} \cdot SIF(10\%)(kW) = 15333.58 \cdot 10\% = 1533\ kW \tag{6.7}$$

$P_{available}$ is the extraction limit, i.e. the power that can be extracted from the selected site without significant economic or environmental effects.

Farm method

The farm method for estimating energy extraction using tidal stream farms is based on the concept of an array of tidal stream devices, each of which extracts an amount of energy related to the incoming energy. The resulting extracted energy is therefore purely dependent on the size and number of the devices, conversion efficiency and the packing density within the site area.

The aim of comparing the two methods is to assess how much power is extracted from the sea. Consequently, the electrical power has to be divided by the power take-off efficiency ($\eta_{POWERTAKE\text{-}OFF}$) as the powertrain losses will be returned to the sea as heat energy rather than as kinetic energy.

To estimate the resource at a site with the farm method, the number of turbines that can be installed should be determined.

Considering the mean electrical net power that each turbine can generate, P_{mean} = 84 kW, obtained at the initial selected site (x: 15, y: 80) in *Table 6.2*, and dividing it by its $\eta_{POWERTAKE\text{-}OFF}$ = 89.4%, results in a power value of 94 kW, which is the gross power extracted from the sea by a single TEC turbine (P_{exTEC}) necessary to generate 84 kW of net power. The number of turbines (N_T) that can be installed is calculated dividing the extraction limit by the gross power extracted by a single TEC turbine:

$$N_T = \frac{P_{avilable}}{P_{exTEC}} = \frac{1533}{94} \approx 16\ turbines \tag{6.8}$$

Figure 6.7 displays the proposed tidal array configuration for the selected site, taking into account the recommendations on device spacing and farm layout described previously.

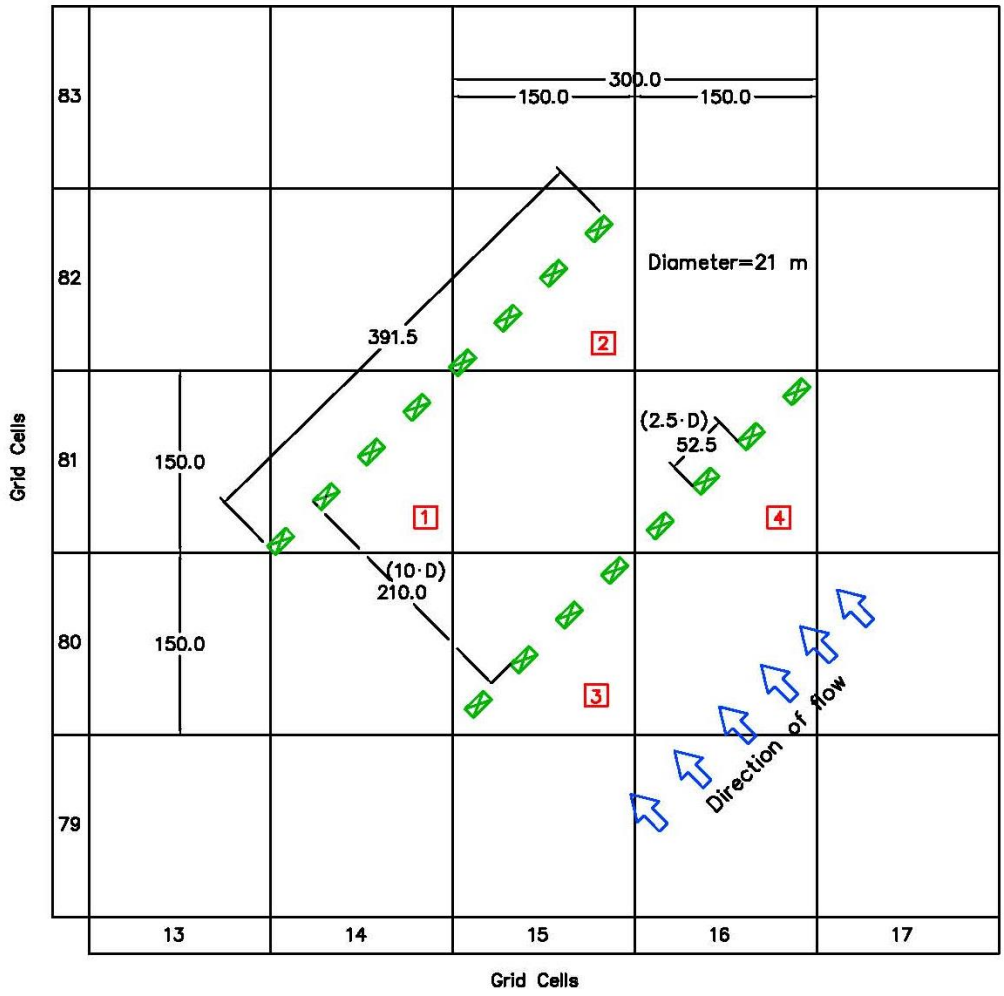

Figure 6.7: Proposed tidal farm deployment composed by 16 TEC turbines of 21 m diameter. Distances are in metres

The mean electrical power (P_{mean}) has been assessed (*Table 6.2)* for each device in each grid cell, where a velocity distribution has been calculated.

The total resource estimated by the farm method has been obtained simply by the sum of P_{mean} divided by $\eta_{POWERTAKE\text{-}OFF}$ of each device that can be installed in the area. In the following equation *n* is an index that represents a TEC turbine.

$$P_{farm} = \sum_{n=1}^{N_T} P_{mean\,(n)} / \eta_{POWER\ TAKE-OFF(n)}\ \ (kW) \tag{6.9}$$

P_{farm} has been calculated for each device obtaining the total energy generated by the tidal array as shown in *Table 6.5:*

	x	y	$P_{mean}/\eta_{powertake-off}$ (kW)	N turbines	
Zone 1	14	81	85	4	340.01
Zone 2	15	82	83	4	331.54
Zone 3	15	80	94	4	375.71
Zone 4	16	81	90	4	361.55
			N_T	16	
				P_{farm}	**1409 kW**

Table 6.5: Pf_{arm} calculation of the site selected for TEC turbine array deployment

The available power calculated with the flux method can be compared to the extractable power obtained with the farm method, in order to verify that this last one is not greater than the available power, P_{farm} = 1409 kW < $P_{available}$ = 1533 kW.

Depending on the number of different grid cells for which a velocity distribution is available, each device should be designed with a different rated power to best fit the velocity distribution. This is unlikely to be the best method in practice as economies of scale would normally be lost. Hence, the devices would typically be grouped in areas of similar velocity distributions. In any case, the four zones, or grid cells, considered in the present study have similar velocity distributions; therefore the 16 turbines have also the same rated power with a value of P_{rated} = 241 kW.

The annual energy production for the tidal farm designed in Ría de Vigo has been obtained by combining the P_{farm} with the available hours per year and considering the power take-off efficiency to obtain the net value of production:

$$AEP_{farm} = 8760h \cdot 1409kW \cdot \eta_{POWER\,TAKE-OFF}(90\%) = \ \ 11.12\ GWh \tag{6.10}$$

According to the World Energy Council [65] the average household electricity consumption in Spain is 4222 kWh/year. Therefore the number of homes that could be powered by the tidal farm is around 2630.

6.3. Technology conversion devices

A heartening large number of TEC turbines and different types of devices are being developed. Hereafter the description of two different TEC turbines whose principal specifications [54] are similar to those required in the tidal farm above calculated is included. Despite these devices might not be the latest developments, both are trustable and robust designs that have been contemplated in many feasibility studies [66].

6.3.1. Lunar Energy

Device description

The Lunar Energy technology, known as the Rotech Tidal Turbine (RTT) and illustrated in *Figure 6.8* is a horizontal axis turbine located in a symmetrical duct. The features of the RTT are the utilisation of a fixed duct, a patent pending blade design and the use of a hydraulic speed increaser. The full-scale prototype is designed to produce 1 MW of electricity while the initial commercial unit, the RTT2000, is designed to produce 2 MW. The geometry of the RTT2000 has been used to establish parameters for this project to address critical engineering issues. Ballast and structural reinforcements can be scaled to meet load conditions at the side based on the maximum tidal current speed. The gravity foundation is provided by a concrete base, which can be supplied with additional ballast to meet the required stability in high currents. The duct consists of steel plates which are supported by a steel tubular frame.

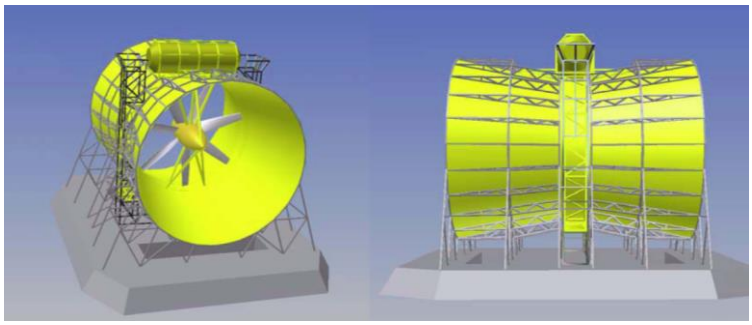

Figure 6.8: Lunar Energy prototype design

A cassette with the complete power take-off, including rotor, hydraulic power conversion, electrical generation and grid synchronization is inserted as a module into the duct (*Figure 6.9*). This arrangement allows for relatively simple removal and replacement of the power conversion system and simplifies operation and maintenance procedures.

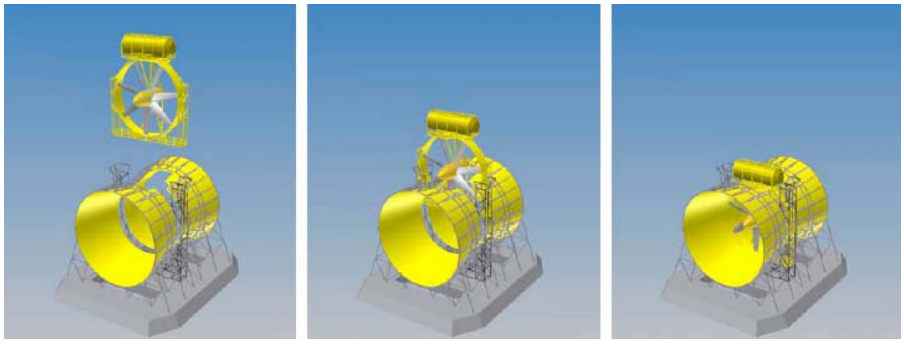

Figure 6.9: Insertion and removal of cassette

Based on the site design velocity the basic design's weight breakdown can be scaled to ensure structural integrity and device stability. *Table 6.6* contains the key properties for the scaled design.

Generic device specifications	
Power conversion	Hydraulic
Electrical output	Synchronised with grid
Foundation	Gravity base
Dimensions	
Duct inlet diameter	21 m
Duct length	27 m
Duct clearance to seafloor	10 m
Duct inlet area	346 m^2
Hub height above seafloor	20.5 m
Weight breakdown	
Structural steel	277 tons
Ballast	332 tons
Total installed dry-weight	609 tons
Power	
Cut-in speed	0.7 m/s
Rated speed	1.57 m/s
Rated power	252 kW

Table 6.6: RTT200 specifications optimized for the selected site conditions. Note that specifications are a scaled version of the device commercial unit, so some characteristics may defer from the designed generic TEC turbine in 6.1

Installation

The device is deployed in two pieces, the concrete base and the duct. The concrete base is constructed on a casting barge in calm and protected waters. The casting barge is then outfitted with four vertical pontoons (3 m long), which are attached to each corner of the barge deck to provide stability during barge submersion. After the base is complete, the barge is ballasted until the deck is about 1.5 m below the water level. This will allow the completed base shell to float free with a draft of about 1.2 m. Once the base is floated off the barge it is sunk to the bottom in a water depth of at least 8 m. Riser pipes are used to control the descent. A transport barge is floated over the base and preinstalled strand jacks are used to lift the base from the seabed until it is directly underneath the barge. The base is then filled with ballast and made ready for deployment. Finally, the barge is towed to its deployment location and the same strand jacks are used to lower the base to its prepared seabed.

Both the duct and the cassette unit are guided into the final position using pre-installed guide wires extending vertically from the base structure to beams extending out in front of a derrick barge. The derrick barge places the duct onto a frame attached to the front of the barge. The duct is then attached to the guide wires and the guide wires are tensioned. Finally the duct is lowered onto the base using strand jacks and guide wires.

After set down, a remote operated vehicle (ROV) will disconnect strand jacks and guide wires from the base and duct.

The same procedure can be used to deploy and recover the cassette. The only difference is that the cassette weighs less and as a result a smaller (and less costly) derrick barge can be used.

Scour protection (if required) can be provided by either using concrete infill below the base or by placing articulated concrete mats onto the seabed.

Most installation and maintenance activities can be carried out from a derrick barge.

Operational and maintenance activities

The operational and maintenance (O&M) philosophy of Lunar Energy's RTT2000 is to provide a reliable design that would require a minimal amount of intervention over its lifetime. In order to accomplish this, highly reliable and proven components are used even if that means lower power conversion efficiency and performance as a result.

All of the power conversion equipment of the RTT2000 is mounted on a cassette, which can be removed from the duct and brought into a port to carry out O&M activities. The fact that the device is completely submersed makes its operation very dependent on attaining claimed reliability as each repair requires the recovery of the duct which requires specialized equipment. Lunar Energy has addressed this issue by optimizing its O&M strategy for minimal intervention. It is expected that the cassette is swapped out every 4 years. The critical components susceptible to failure in the power conversion system are the hydraulic ones. Given the high cost for maintenance intervention, the reliability of the system becomes a critical attribute, which will need to be proven on a prototype system.

6.3.2 Marine Current Turbines (MCT)

Device description

The MCT SeaGen consists of two horizontal axis rotors and powertrains (gearbox, generator) attached to a supporting monopile by a cross-arm (*Figure 6.10*). The monopile is installed through surface drilling and includes an integrated lifting mechanism to pull the rotors and power trains out of the water for maintenance access. Rotors have full span pitch control and drive induction generators at variable speed through three stage gearboxes. Generators and gearboxes are submersible devices whose casings are exposed directly to the passing sea water for efficient cooling. A patented and important feature of the technology is that the entire wing, together with the rotors, can be raised up the pile above the water surface for maintenance. Blade pitch is rotated 180º at slack water to accommodate bidirectional tides without requiring a separate yaw control mechanism.

Figure 6.10: MCT SeaGen at operation (left) and maintenance (right)

A 1.2 MW prototype SeaGen is intended as a commercial prototype and incorporates important learning from SeaFlow, a 300 kW single rotor test rig, which has been in operation for about 3 years. SeaFlow tested many of the features of SeaGen and has helped the design process by providing large amounts of data.

While in principle SeaGen is scalable and adaptable to different site conditions, for the present study, the 18 m dual rotor version has been proposed to optimise the system to local site conditions to estimate device cost parameters. The deployment in Ria de Vigo is sufficiently large that could accept surface piercing SeaGen technology. Turbines could be placed in such a way that they clearly mark the channel and actually increase the safety of passing boats at the site. *Table 6.7* contains the key properties for the scaled design.

Generic device specifications	
Speed increaser	Planetary gear box
Electrical output	Synchronised to grid
Foundation	Monopile drilled and grouted into bedrock
Dimensions	
Pile length	68 m
Pile diameter	3.5 m
Rotor Diameter	18 m
Rotors per SeaGen	2
Hub height above Seafloor	17 m
Weight breakdown	
Monopile	115 tons
Cross arm	55 tons
Total steel weight	170 tons
Performance	
Cut-in speed	0.7 m/s
Rated speed	1.61 m/s
Rated electric power	457 kW

Table 6.7: SeaGen specifications optimized for the selected site conditions. Note that specifications are a scaled version of the device commercial unit, thus some characteristics might defer from the designed generic TEC turbine in 6.1

Installation

MCT proposes to install their large diameter monopoles (3.5 m – 4 m outer diameter) using a jack-up barge. This is consistent with other European offshore wind projects that have used such barges to deploy offshore wind turbine foundations. If jack-up barges are not available there are a significant number of crane barges available from which the installations of these piles could be carried out. Typically installation projects include the construction of bridges, cofferdams and pile installations. Crane capacities vary with some of the largest derrick barges being able to lift up to 600 tons. To carry out the installation of these relatively large 3.5 m diameter piles, it was determined that a crane capacity of about 400 tons or more would be adequate to handle the piles, drilling bits and other installation equipment. Several options exist for installing piles: driving piles using hydraulic hammer, combination of water jetting and vibratory hammer, drill and connect a sleeve and then grout the pile in the place, etc. Each of these methods has advantages and disadvantages. A drilled pile installation would involve drilling into the consolidated sediments and stabilising the walls of the drill hole with metal sleeve. Once the hole has been drilled to a suitable depth, the pile is inserted and grouted into place. This method of installation is preferred by MCT to limit excessive pile fatigue during the installation process and drilling is required in most locations because of bedrock presence that would need to be penetrated.

Operational and maintenance activities

The guiding philosophy behind MCT design is to provide low cost access to critical turbine systems. Since an integrated lifting mechanism on the pile can lift the rotor and all subsystems out of the water, general maintenance activities do not require specialised ships or personnel (divers). The overall design philosophy appears to be that the risks associated with long-term underwater operation are best offset by simplifying scheduled and unscheduled maintenance tasks. The only activity that could require use of divers or ROVs would be repairs to the lifting mechanism or inspection of the monopole, none of which are likely to be required over the project life.

Annual inspection and maintenance activities are carried out using a small crew of two or three technicians on the device itself. Tasks involved in this annual maintenance cycle include activities such as: replacement of gearbox oil, applying bearing grease and changing oil filters. In addition, all electrical equipment can be checked during this inspection cycle and repairs carried out if required. Access to the main structure can be carried out safely using small craft as a rigid inflatable boat in most sea conditions.

For repairs on larger subsystems such as the gearbox, the individual components can be hoisted out with a crane or winch and placed onto a motorised barge. The barge can then convey the systems ashore for overhaul, repair or replacement. For the purpose of estimating the likely O&M cost, the mean time to failure was estimated for each component to determine the resulting annual operational and replacement cost. Based on wind turbine data, the most critical component is the gearbox which shows an average mean time to failure of 10.8 years.

6.4. Economical approach

The cost assessment for the tidal farm designed in 6.2 has been carried out by taking data provided by the manufacturer MCT with the aim of calculating the approximate capital cost breakdown of a tidal plant deployed in the selected site. The main factors that influence the relative economic cost at a particular site are:

Design current speed: the maximum velocity of the water expected to occur at the site. The cost of the structural elements is related to the structural loads produced by the current velocity. For a conservative approach, design velocity is set to the site's peak, rather than to the device rating, in order to simulate the loads experienced during runaway operation in the event of pitch control failure.

Velocity distribution: obtained in section 6.1, it shows the tidal stream velocities at which there is a useful number of reoccurrence to pay for the capital cost which is needed to tap into this velocity bin.

Seabed composition: has an important impact on the foundation design of the TEC turbine. For a monopile foundation the seabed composition determines the installation process and consequently it impacts the cost of the monopile.

Number of installed turbines: in general larger number of units will result in lower cost of electricity. Infrastructure cost required to interconnect the devices to the electric grid can be shared and therefore their cost per unit of electricity produced is lower. Installation cost per turbine is lower because mobilisation cost can be shared between multiple turbines. In addition, the first unit is more expensive than subsequent units as the installation contractor is able to increase their operational efficiency.

Device reliability and O&M procedures: reliability directly impacts the operation and maintenance cost of a device. O&M costs are particularly uncertain since no tidal current turbine has been in service for extended periods of time.

Insurance cost: it varies depending on the risk of the project. While this is an area of uncertainty, as the industry is still in a nascent state, it has been assumed that a commercial farm will incur in insurance costs similar to mature offshore projects, which is typically about 1.5% of the installed cost.

The following table shows the cost breakdown for the TEC turbine farm at the deployment site. The cost of each component (€/kW) has been extracted from data from other projects provided by MCT [54]. The installation of 16 turbines at the site has been considered, each one with a rated capacity of 241 kW and with a power coefficient C_p = 0.32, delivering a total of 11.12 GWh per year of electrical output.

	€/kW	€/turbine	€/Farm	in %
Power conversion system	745	179,483	2,871,732	24.0%
Structural elements	572	137,800	2,204,808	18.4%
Subsea cable cost	103	24,743	395,891	3.3%
Turbine installation	927	223,450	3,575,199	29.9%
Subsea cable installation	746	179,674	2,874777	24.0%
Onshore electric grid interconnection	12	2,777	44,424	0.4%
Total installed cost	**3,103**	**747,927**	**11,966,831**	**100%**
O&M cost	61	14,656	234,489	56.6%
Annual insurance cost	47	11,219	179,502	43.4%
Total annual O&M cost	**107**	**25,874**	**413,992**	**100%**

Table 6.8: TEC turbine plant capital cost breakdown

Hereafter a basic analysis of the project profitability is included. An investment is profitable when its yield values are greater than the resources utilised.

There are some profitability indicators to evaluate the economic yields of installing TEC turbines. For the present assessment, to determine the profitability of the investment, the Internal Rate of Return (IRR) and the PAYBACK period have been taken into consideration.

The IRR is the interest rate at which the Net Present Value (NPV) of all the cash flows from a project or investment equals zero. The IRR is used to evaluate the attractiveness of a project or investment. An investment is considered acceptable if its internal rate of return is greater than an established minimum acceptable rate of return or cost of capital.

The PAYBACK period, is the length of time required to recover the cost of an investment.

Table 6.9 shows the financial assumptions taken into account for analysing the profitability of the project:

Investment cost	11,966,830.50	€
Income of the project	888,563.77	€
Yearly maintenance and operation expenses	413,991.68	€
Inflation rate	3.00%	
Nominal interest rate	3.00%	
Lifespan of the project	30	years
Annual Energy Production farm (AEP_{farm})	11,107.05	MWh
Tariff for electricity supplied by MCT in Spain	80	€/MWh

Table 6.9: Financial considerations

The resulting IRR at the end of the lifespan is 1.16% and the investment cost may be recovered (PAYBACK return) at a minimum period of 26 years.

Both results prove the immaturity of the TEC technology. While the investment cost is recovered before the end of the lifespan, PAYBACK values lower than 12 years are desired to assure the profitability of the project. Even if the IRR value is positive, it is lower than the normal nominal interest rate and thus it is still a bit far from being attractive for project investing.

Profitability will be improved if the necessary investments are made in TEC technology design in order to enhance the efficiency of the turbines, which will increase the energy production and will raise the income. The investment cost of this kind of projects is still very elevated. Research in optimisation of installation methods should be promoted for the purpose of reducing investment costs.

The results of this economic assessment may help government policy makers determine the public benefit of investing in tidal power plants. Such technology support is typically done through funding R&D and through incentives for the deployment of targeted renewable technologies.

This emerging technology still requires large investment in development to improve its efficiency in order to become a competitive technology for renewable energy production.

6.5. Environmental approach

By their nature, tidal stream devices are designed to extract energy from the water, and their presence will affect the physical, chemical and ecological features of the marine environment [67]. This section provides an overview of the main environmental impacts and some of the key issues in dealing with the potential effects of tidal energy development on the marine environment.

The key environmental impacts from tidal stream development are those related to ecology (habitats and species), landscape and seascape, noise (airborne and underwater), seabed, sediments and currents, and water quality [68].

Impacts on other users of the marine environment, such as fishing and navigation, will also need to be considered as part of an environmental impact assessment. In practice, these issues need to be considered much earlier at a strategic level and in the site selection.

Environmental impacts at the various stages of development should be contemplated [69], including:

Construction: the key impacts will be related to drilling and piling activities, increased levels of noise, and increased activity and pollution risk associated with construction boats and activity. Direct effects on the seabed are greatest at this stage. For tidal

stream devices, construction of the device itself would usually take place onshore, followed by installation of the device and associated cabling at sea.

Operation and maintenance: the device may have effects on water movements and sediment, as energy is extracted from the tidal flows, and underwater noise and the turbine operation have the potential to affect ecology, fish and marine mammals. Tidal stream devices, once developed to full scale, can be expected to have a lifetime of around 30 years.

Decommissioning: similar effects to those identified for commissioning can be expected. Further effects at this point may include disturbance to any new community of marine organisms that has become established on the device. The environmental effects of associated onshore infrastructure, in particular power cabling, will also need to be taken into account, and can often be a significant practical issue during consenting (as separate planning consent must be sought).

6.5.1. Ecology (habitats and species)

A number of marine species and habitats in Galician coastal waters have the potential to be affected by tidal energy schemes. These include birds, fish, marine mammals, plankton, and benthic communities on the seabed. Terrestrial habitats may also be affected by infrastructure works to accommodate the landward transmission of electricity. The main issues affecting habitats arise from changes in the physical environment, for example, changes in water flow and tidal mixing, wave action, tidal inundation, patterns of sedimentation and erosion, and disturbance of the seabed by construction and cabling. These changes can alter the character of marine communities, or lead to the displacement of species from feeding or breeding areas. Fish and marine mammals may be particularly affected by the generation of underwater noise, and the electromagnetic fields generated by sub-sea transmission cables. Collision risk is another factor that will need to be considered for each device. Although the risk from turbines turning slowly underwater may be low, this risk, and the potential behavioural changes of these species, will need to be assessed with care, and monitoring of installed test devices will be needed. There are also potentially positive effects from tidal stream development for nature conservation. A tidal installation may function as a refuge area for fish populations as a result of reduced fishing pressure from the creation of ‘no-catch’ zones. The potential benefits of this will depend on the specific impacts of a device, the scale of its deployment, and consideration of decommissioning implications, but this may offer an opportunity to integrate renewable energy generation (and a commercial activity) with nature conservation objectives.

6.5.2. Landscape and seascape

Many coastal areas have an important amenity and natural heritage value for communities, visitors, and recreational users. The placement of a tidal energy scheme in waters close to the shore may have an impact on the landscape and seascape of the

area, particularly where the devices are surface-drilling structures, as SeaGen technology. The level of impact will depend on the landscape character of the coastal area and the type of tidal energy scheme.

Visual effects, both the appearance of a device and its visibility from land or from a vessel, and the impacts on landscape and seascape are often a key issue for local communities, and design and location will need to be considered. While tidal stream development is likely to have a lower visual impact than wind development, lessons can be drawn from that industry about the importance of early engagement on these issues with local communities. In the case of a new technology, this may mean providing good information to demonstrate the very low visibility of a device or development. The visual effects of supporting infrastructure (substations, pylons) will also be a key issue.

6.5.3. Noise

Noise and vibrations travel significant distances underwater. Increases to background noise during construction and operation may have serious effects on marine mammals and fish, depending on the level, frequency and duration of noise. Again, this is an area where there is insufficient information on the potential effects of noise levels from tidal stream devices. Depending on the distance from shore, climatic conditions and wind direction, noise from construction, maintenance and decommissioning activities may also affect local communities.

6.5.4. Seabed, sediments and current

The placement of tidal energy structures and their associated cabling on the seabed will result in a change in the physical features of the area, and may involve a loss of habitats. Fixed tidal stream devices will have a relatively small footprint for each individual device, varying in accordance with whether the device is fixed or floating. For an array of tidal devices, cabling arrangements will be complex, effectively increasing the footprint of an installation. Cabling may have a significant but short-term adverse impact on the seabed. At the decommissioning stage, cabling may be left in place to avoid further disturbance, or re-used with a new installation of devices. The placement of a solid structure on the seabed in an area of strong tidal flows will affect patterns of sediment erosion, transportation and deposition. By extracting energy from the flow, a tidal stream device can reduce the downstream velocity of the turbine considerably, with the effects discernible some distance away. This is one of the key areas where the potential cumulative effects of deploying tidal stream devices in large arrays are unknown and further research will be required.

6.5.5. Water quality

The main issues for water quality from tidal stream development are the potential leakage of lubricants and hydraulic fluids, and the chance that increased volume of vessel traffic associated with the scheme may result in increased levels of fuel and oil leakage into the water.

6.5.6. Design and mitigation measures

Relative to tidal barrages and lagoons, tidal stream devices are expected to have relatively low effects on the environment. This will depend on the type and number of devices deployed. The greatest environmental effects can be expected to occur where arrays, farms or a series of farms are deployed. Possible mitigation methods for managing effects on the seabed, sediments and hydrodynamics include sensitive design of base structures and choice of the location to minimise impact on sensitive sites. The design of devices will also need to consider their interaction with fish, birds and marine mammals. It may also be possible to time construction and decommissioning activities to minimise adverse impacts on sensitive ecological receptors (such as marine mammals affected by noise). Monitoring of test device installations will improve the understanding of ways in which impacts can be avoided or minimised.

Chapter VII

Conclusions and future work

Tidal current energy, which harnesses the kinetic energy contained in the tidal streams, is emerging as a great potential energy source. It has a number of advantages with regard to other renewable energies. The resource predictability, the minimal visual impact and land occupation, its high load factor, its sustainability, etc. are some of the noteworthy features.

The Ría de Vigo, a large coastal embayment located in the north-west of Spain, seems to be an attractive location for evaluating the capability of tidal current power production.

In order to quantify the tidal current power potential in the Ría de Vigo and to assess the feasibility of a tidal plant, a numerical model, vertically averaged (2DH), was implemented to simulate the hydrodynamics of the embayment. To verify the suitability of the modelled data, the numerical model was successfully calibrated by comparing model data with field campaign measurements conducted in the area of application. Further studies should consider the implementation of a 3D model in order to enhance the accuracy of the simulations, especially concerning the variation of velocities between the water surface and the device's hub height.

The numerical model was applicable for the assessment of the tidal stream power capacity of the Ría de Vigo. The area of study proved to be a suitable zone comprising velocities beyond 2 m/s. The highest tidal current occurred in the outer part of the ría, in the strait between Cíes Islands and the northern peninsula, with a maximum value of 2.5 m/s at mid-flood of a mean spring tide. The velocity magnitudes in the study area were higher during the flood than during the ebb. The power density reached its maximum with a value of 7.5 kW/m^2 at mid-flood of a mean spring tide.

The selection of the best tidal energy exploitation site was made representing the average power density of an entire tidal cycle. The selected location was the site that provided the highest power output for a tidal cycle, taking into account the average power density and the installable size of the rotor's diameter, which depends on the local bathymetry.

The chosen site for TEC turbine deployment was located at 42°15'16.7"N 8°53'23.9"W coordinates, at approximately 1.2 km from the Costa da Vela (at the peninsula) and at 1.7 km from the Cíes Islands. Certainly, the site offered adequate space to allow ship navigation along the strait, as well as ensured easy transport of electricity, because the location is considered a near-shore site.

The velocity and power magnitudes obtained at the selected site during the mean spring peak were V_{msp} = 2.2 m/s and P_{msp} = 5.45 kW/m^2, and during an entire tidal

cycle (average values) *AVM* = 0.89 m/s and *APD* = 0.77 kW/m^2. The annual energy available at the site resulted in 6.71 MWh/m^2.

To apply the analysis of the tidal resource to a practical study-design of a tidal farm in the Ría de Vigo it was decided to consider a generic TEC turbine and not to select any specific device. As no single tidal stream technology is currently established, generic or standard, the horizontal axis tidal current turbine (HATCT) was assumed for all the calculations within the farm design process.

A generic turbine of 21 m diameter was contemplated since the selected site offered enough depth to fit that turbine dimension. The principal parameters of the generic TEC turbine calculated are: $V_{cut\text{-}in}$ = 0.5 m/s, V_{rated} = 1.56 m/s, P_{rated} = 241 kW, *Annual Energy Production* = 735 MWh and power coefficient C_p = 0.32.

Note that performance and energy conversion yields could be improved by the implementation of a specific adjusted device designed for the site and its unique requirements. Tidal turbine developers offer device efficiency curves of power conversion systems that can be used to find the most optimal design for the study area, albeit the efficiency curves cannot be applied to all locations. Further development in turbine efficiency is the key element to impulse tidal energy technology to reach the commercial stage and become a competitive renewable energy resource. Future work should be done in order to enhance the turbines' capacity of energy capture, i.e. to achieve turbines working at velocities below the cut-in speed or over the rated velocity.

As there is no standard methodology to design a turbine farm and considering the prefeasibility character of the study here-in, an array configuration was proposed to describe the resource and to give a conceptual idea on methodology farm design.

The turbine array consisted in 16 horizontal axis turbines displayed in two rows (2 x 8) at the selected site and surroundings, facing the main tidal stream direction. The array distribution was made according to the lateral and downstream spacing recommendations in order to avoid negative hydrodynamic interaction effects on the turbines. The available energy resource is not fully extractable due to environmental concerns; therefore an extraction limit (*SIF*) of 10% was imposed to ensure no significant alteration of the flow speed.

Each of the 16 turbines within the array had a rated power with a value of P_{rated} = 241 kW. Considering the mean power produced by each turbine, the annual energy production for the tidal farm designed in Ría de Vigo was AEP_{farm} = 11.12 GWh. Taking into consideration the average household electricity in Spain, the number of homes that could be powered by the tidal farm is around 2630, which is a proper value.

The cost assessment of the tidal farm was carried out by taking data provided by the manufacturer MCT with the aim of calculating the approximate capital cost breakdown of a tidal plant deployed in the selected site. The total investment cost resulted in approximately 12 M€. A basic analysis of the profitability of the project was made in order to give a qualitative impression for future investments comparisons. It proved to be non-cost-effective for a commercial plant scheme. The investment cost of this kind of projects is still very elevated. O&M costs are really high due to the remote and harsh environment in which it operates.

Research in installation and transportation methods should be encouraged. There are some innovative inventions such as folding tidal turbines [70], albeit still prototypes; they act as an alternative device design with the aim of reducing the total cost and the installation time.

Cost-reduction can be achieved through a series of mechanisms that fit with the continuous development of tidal energy technologies. Device performance improvement, up-scaling, experience and innovation are the key stones that will allow tidal technology to become commercially viable and to achieve increased rate of deployment.

Moreover, further work needs to be carried out in order to provide answers to several uncertainties regarding device spacing and available extractability of the resource. Could the device spacing be narrower, reducing farms' footprint, without deteriorating individual device performance? Is the *SIF* coefficient too conservative for the study here-in? Research should be promoted in this topic to determine the real amount of resource that could be extracted without harming the marine environment.

Regarding to the environmental approach, stream devices are designed to extract energy from the water, which affects the physical, chemical and ecological features of the marine environment. The main environmental impacts were discussed taking into account the various stages of development, construction, O&M, and decommissioning. The greatest environmental effects are expected to potentially occur where farms are deployed. Possible mitigation methods for managing effects on the seabed, sediments and hydrodynamics include sensitive design of base structures and choice of location to minimise impact on sensitive sites, as well as consideration of the farm interaction with the marine fauna. Monitoring of test device installations would improve the understanding of ways in which impacts can be avoided or minimised. In general, tidal stream devices are expected to have relatively low effect on the environment compared with other renewable technology as wind and solar farms or hydroelectric power plants.

Tidal energy is a promising renewable energy source available in the Galician coast, specifically in the Ría de Vigo. The results of this study may encourage the government and other institutions to promote investment on research for design, develop, construct and deploy TEC turbines in order to become competitive technology for renewable energy production.

Chapter VIII

References

[1] Energy Information Administration (EIA), “World energy consumption will increase 56% by 2040.” [Online]. Available: http://www.eia.gov/todayinenergy/. [Accessed: 11-Feb-2015].

[2] Asociación de Empresas de Energías Renovables (APPA), “La energía en España.” [Online]. Available: http://www.appa.es/index.php. [Accessed: 11-Feb-2015].

[3] EUR-Lex, “2009/28/EC Directive.” [Online]. Available: http://eur-lex.europa.eu/legal-content/en/ALL/?uri=CELEX:32009L0028. [Accessed: 11-Feb-2015].

[4] Ministry of Industry Energy and Tourism of Spain, “Spain’s national renewable energy action.” [Online]. Available: http://www.feed-in-cooperation.org. [Accessed: 10-Jan-2015].

[5] Ministry of Industry Energy and Tourism of Spain, “Energy in Spain 2013.” [Online]. Available: http://www.minetur.gob.es/energia/en-us/Paginas/Index.aspx. [Accessed: 05-Jan-2015].

[6] S. Barbarelli, G. Florio, M. Amelio, N. M. Scornaienchi, A. Cutrupi, and G. Lo Zupone, “Design procedure of an innovative turbine with rotors rotating in opposite directions for the exploitation of the tidal currents,” *Energy*, vol. 77, pp. 254–264, 2014.

[7] H. Faez, A. El-shafie, and O. A. Karim, “Tidal current turbines glance at the past and look into future prospects in Malaysia,” *Renew. Sustain. Energy Rev.*, vol. 16, no. 8, pp. 5707–5717, 2012.

[8] Instituto para la Diversificación y Ahorro de la Energía (IDAE), “2011-2020 Renewable Energy Plan.” [Online]. Available: http://www.idae.es/index.php/id.670/relmenu.303/mod.pags/mem.detalle. [Accessed: 05-Jan-2015].

[9] F. O. Rourke, F. Boyle, and A. Reynolds, “Tidal energy update 2009,” *Appl. Energy*, vol. 87, no. 2, pp. 398–409, 2010.

[10] A. S. Bahaj, “Generating electricity from the oceans,” *Renew. Sustain. Energy Rev.*, vol. 15, no. 7, pp. 3399–3416, 2011.

[11] Atlantis Resources, “Technology comparison between offshore wind turbines and tidal turbines.” [Online]. Available: http://atlantisresourcesltd.com/marine-power/technology-comparison.html. [Accessed: 05-Jan-2015].

[12] Y. Li, “On the definition of the power coefficient of tidal current turbines and efficiency of tidal current turbine farms,” *Renew. Energy*, vol. 68, pp. 868–875, Aug. 2014.

[13] R. Carballo, G. Iglesias, and A. Castro, “Numerical model evaluation of tidal stream energy resources in the Ría de Muros (NW Spain),” *Renew. Energy*, vol. 34, no. 6, pp. 1517–1524, 2009.

[14] “What is OTEC -OTEC news.” [Online]. Available: http://www.otecnews.org/what-is-otec/. [Accessed: 03-May-2015].

[15] G. Iglesias, M. López, R. Carballo, A. Castro, J. A. Fraguela, and P. Frigaard, “Wave energy potential in Galicia (NW Spain),” *Renew. Energy*, vol. 34, no. 11, pp. 2323–2333, 2009.

[16] J. P. Sierra, C. Mösso, and D. González-Marco, “Wave energy resource assessment in Menorca (Spain),” *Renew. Energy*, vol. 71, pp. 51–60, 2014.

[17] J. P. Sierra, D. González-Marco, J. Sospedra, X. Gironella, C. Mösso, and A. Sánchez-Arcilla, “Wave energy resource assessment in Lanzarote (Spain),” *Renew. Energy*, vol. 55, pp. 480–489, 2013.

[18] “Introduction to Tides.” [Online]. Available: http://wegc203116.uni-graz.at/meted/oceans/tides_intro/print.htm. [Accessed: 12-May-2015].

[19] B. Nathaniel, “Tides and Tidal Current,” *Am. Pract. Navig.*, p. 896, 2002.

[20] “Misconceptions about tides.” [Online]. Available: https://www.lhup.edu/~dsimanek/scenario/tides.htm. [Accessed: 05-May-2015].

[21] “Ocean Tides.” [Online]. Available: http://www.physicalgeography.net/fundamentals/8r.html. [Accessed: 05-May-2015].

[22] “Tidal Bulges.” [Online]. Available: http://galleryhip.com/tidal-bulges.html. [Accessed: 05-May-2015].

[23] D. Murphy, “Excavations of a Mill at Killoteran, Co. Waterford as Part of the N-25 Waterford By-Pass Project,” University College Dublin and National Roads Authority, 2005.

[24] R. Dorf, *The Energy Factbook*. New York, 1981.

[25] “La Rance Barrage - Wyre Tidal Energy.” [Online]. Available: http://www.wyretidalenergy.com/tidal-barrage/la-rance-barrage. [Accessed: 05-May-2015].

[26] “Tidal power | energy | Encyclopedia Britannica.” [Online]. Available: http://global.britannica.com/EBchecked/topic/595132/tidal-power. [Accessed: 06-May-2015].

[27] “Ocean Current Energy | BOEM.” [Online]. Available: http://www.boem.gov/Renewable-Energy-Program/Renewable-Energy-Guide/Ocean-Current-Energy.aspx. [Accessed: 06-May-2015].

[28] T. Montllonch, “Master thesis TIDAL POWER : Economic and Technological assessment,” Tsinghua University.

[29] J. Khan and G. S. Bhuyan, “Global Technology Development Status, Report prepared by Powertech Labs for the IEA-OES,” 2009. [Online]. Available: www.powertechlabs.com.

[30] “Tidal devices. EMEC (European Marine Energy Centre).” [Online]. Available: http://www.emec.org.uk/marine-energy/tidal-devices/. [Accessed: 08-May-2015].

[31] S. T. López, R. A. Varela, and E. Delhez, “Residual circulation and thermohaline distribution of the Ría de Vigo : a 3-D hydrodynamical model,” *Sci. Mar.*, vol. 65, pp. 277–289, 2001.

[32] LIM, “Desarrollo de un sistema operacional de predicción de Corrientes y agitación de alta resolución para el Puerto de Vigo,” Research Report, Laboratori d’Enginyeria Marítima, Universitat Politècnica de Catalunya, 2011.

[33] D. B. Haidvogel, H. Arango, W. P. Budgell, B. D. Cornuelle, E. Curchitser, E. Di Lorenzo, K. Fennel, W. R. Geyer, A. J. Hermann, L. Lanerolle, J. Levin, J. C. McWilliams, A. J. Miller, A. M. Moore, T. M. Powell, A. F. Shchepetkin, C. R. Sherwood, R. P. Signell, J. C. Warner, and J. Wilkin, “Ocean forecasting in terrain-following coordinates: Formulation and skill assessment of the Regional Ocean Modeling System,” *J. Comput. Phys.*, vol. 227, pp. 3595–3624, 2008.

[34] Georgia Tech Reserch Corporation, “Assessment of Energy Production Potential from Tidal Streams in the United States. Final Project Report. Award Number : DE-FG36-08GO18174,” pp. 1–109, 2011.

[35] A. F. Shchepetkin and J. C. McWilliams, “The regional oceanic modeling system (ROMS): a split-explicit, free-surface, topography-following-coordinate oceanic model,” *Ocean Model.*, vol. 9, no. 4, pp. 347–404, 2005.

[36] E. Blayo and L. Debreu, “Adaptive Mesh Refinement for Finite-Difference Ocean Models: First Experiments,” *J. Phys. Oceanogr.*, vol. 29, no. 6, pp. 1239–1250, 1999.

[37] L. Debreu, C. Vouland, and E. Blayo, “AGRIF: Adaptive grid refinement in Fortran,” *Comput. Geosci.*, vol. 34, pp. 8–13, 2008.

[38] J. C. Warner, W. R. Geyer, and J. A. Lerczak, “Numerical modeling of an estuary: A comprehensive skill assessment,” *J. Geophys. Res. C Ocean.*, vol. 110, no. 5, pp. 1–13, 2005.

[39] C. S. Kim and H.-S. Lim, “Sediment dispersal and deposition due to sand mining in the coastal waters of Korea,” *Cont. Shelf Res.*, vol. 29, no. 1, pp. 194–204, 2009.

[40] M. Grifoll, G. Jordà, A. Borja, and M. Espino, “A new risk assessment method for water quality degradation in harbour domains, using hydrodynamic models.,” *Mar. Pollut. Bull.*, vol. 60, no. 1, pp. 69–78, 2010.

[41] Regional Ocean Modeling System, “ROMS.” [Online]. Available: https://www.myroms.org/. [Accessed: 12-Feb-2015].

[42] P. Cerralbo, M. Grifoll, M. Espino, and J. López, “Predictability of currents on a mesotidal estuary (Ria de Vigo, NW Iberia),” *Ocean Dyn.*, vol. 63, no. 2–3, pp. 131–141, 2013.

[43] M. Benbouzid, J. A. Astolfi, S. Bacha, J. F. Charpentier, M. Machmoum, T. Maitre, and D. Roye, *Marine Renewable Energy Handbook*. 2001.

[44] A. N. Gorban, A. M. Gorlov, and V. M. Silantyev, “Limits of the Turbine Efficiency for Free Fluid Flow,” *J. Energy Resour. Technol.*, vol. 123, no. 4, pp. 311, 2001.

[45] W. M. J. Batten, A. S. Bahaj, A. F. Molland, and J. R. Chaplin, “Experimentally validated numerical method for the hydrodynamic design of horizontal axis tidal turbines,” *Ocean Eng.*, vol. 34, no. 7, pp. 1013–1020, 2007.

[46] R. Vennell, “Exceeding the Betz limit with tidal turbines,” *Renew. Energy*, vol. 55, pp. 277–285, 2013.

[47] C. J. Lawn, “Optimization of the power output from ducted turbines,” *Proc Inst Mech Eng A-J Power Energy*, vol. 217, pp. 107–118, 2003.

[48] A. S. Bahaj, A. F. Molland, J. R. Chaplin, and W. M. J. Batten, “Power and thrust measurements of marine current turbines under various hydrodynamic flow conditions in a cavitation tunnel and a towing tank,” *Renew. Energy*, vol. 32, no. 3, pp. 407–426, 2007.

[49] L. S. Blunden and A. S. Bahaj, “Tidal energy resource assessment for tidal stream generators,” *Proc Inst Mech Eng A-J Power Energy*, vol. 221, pp. 137–146, 2007.

[50] C. Legrand, Black and Veatch, and EMEC, *Assessment of Tidal Energy Resource*, 2009.

[51] J. N. Goundar and M. R. Ahmed, “Design of a horizontal axis tidal current turbine,” *Appl. Energy*, vol. 111, pp. 161–174, 2013.

[52] L. Myers and A. S. Bahaj, “Simulated electrical power potential harnessed by marine current turbine arrays in the Alderney Race,” *Renew. Energy*, vol. 30, no. 11, pp. 1713–1731, 2005.

[53] J. Xia, R. A. Falconer, and B. Lin, “Numerical model assessment of tidal stream energy resources in the Severn Estuary, UK,” *Proc. Inst. Mech. Eng. Part A J. Power Energy*, vol. 224, no. 7, pp. 969–983, 2010.

[54] M. Previsic, B. Polagye, and R. Bedard, “System Level Design , Performance , Cost and Economic Assessment – Massachusetts Muskeget Channel Tidal In-Stream Power Plant,” 2006.

[55] “Lunar energy.” [Online]. Available: http://www.lunarenergy.co.uk/. [Accessed: 22-Apr-2015].

[56] “Marine Current Turbines (MTC).” [Online]. Available: http://www.marineturbines.com/. [Accessed: 20-Apr-2015].

[57] A. S. Bahaj and L. E. Myers, “Fundamentals applicable to the utilisation of marine current turbines for energy production,” *Renew. Energy*, vol. 28, no. 14, pp. 2205–2211, 2003.

[58] G. Hagerman and B. Polagye, “Methodology for estimating tidal current energy resources and power production by tidal in-stream energy conversion (TISEC) devices,” *Electr. Power Res. Inst.*, 2006.

[59] “MeyGen Project.” [Online]. Available: http://www.meygen.com/. [Accessed: 20-Apr-2015].

[60] I. G. Bryden, S. J. Couch, A. Owen, and G. Melville, “Tidal current resource assessment,” *Proceedings of the Institution of Mechanical Engineers, Part A: Journal of Power and Energy*, vol. 221, no. 2. pp. 125–135, 2007.

[61] Y. Li, “On the de finition of the power coefficient of tidal current turbines and efficiency of tidal current turbine farms,” vol. 68, pp. 868–875, 2014.

[62] L. E. Myers and A. S. Bahaj, “An experimental investigation simulating flow effects in first generation marine current energy converter arrays,” *Renew. Energy*, vol. 37, no. 1, pp. 28–36, 2012.

[63] R. Vennell, “The energetics of large tidal turbine arrays,” *Renew. Energy*, vol. 48, pp. 210–219, 2012.

[64] R. Ahmadian and R. A. Falconer, “Assessment of Array Shape of Tidal Stream Turbines on Hydro-environmental Impacts and Power Output.”

[65] “Energy Efficiency Indicators: Household electricty consumption.” [Online]. Available: http://www.worldenergy.org/data/efficiency-indicators/. [Accessed: 20-Apr-2015].

[66] R. Bedard, M. Previsic, B. Polagye, G. Hagerman, and A. Casavan, “North America Tidal In-Stream Energy Conversion Technology Feasibility Study,” *Energy*, 2006.

[67] SuperGen UK Centre for Marine Energy Research, “Large Scale Interactive Coupled Modelling of Environmental Impacts of Marine Renewable Energy Farms.”[Online]. Available: http://www.supergen-marine.org.uk/drupal/content/ukcmer/environmental-impacts-marine-energy-farms. [Accessed: 26-Apr-2015].

[68] V. Ramos, R. Carballo, M. Álvarez, M. Sánchez, and G. Iglesias, “Assessment of the impacts of tidal stream energy through high-resolution numerical modeling,” *Energy*, vol. 61, pp. 541–554, 2013.

[69] SDC (Sustainable Development Commission), M. Kadiri, R. Ahmadian, B. Bockelmann-Evans, W. Rauen, and R. Falcone, “Turning the tide,” *A Rev. potential water Qual. impacts tidal Renew. energy Syst. Renew Sust Energ Rev*, 2007.

[70] W. H. Lam and A. Bhatia, “Folding tidal turbine as an innovative concept toward the new era of turbines,” *Renewable and Sustainable Energy Reviews*, vol. 28. pp. 463–473, 2013.